Liver Fatty Acid-Binding Protein Colocalizes with Peroxisome Proliferator Activated Receptor α and Enhances Ligand Distribution to Nuclei of Living Cells†

Huan Huang,‡ Olga Starodub,§ Avery McIntosh,‡ Barbara P. Atshaves,‡ Gebre Woldegiorgis,|| Ann B. Kier,§ and Friedhelm Schroeder*,‡

Department of Physiology and Pharmacology, Texas A&M University, College Station, Texas 77843-4466, Department of Biochemistry and Molecular Biology, Oregon Graduate Institute of Science and Technology, Beaverton, Oregon 97006-8921, and Department of Pathobiology, Texas A&M University, College Station, Texas 77843-4467

Received July 14, 2003; Revised Manuscript Received December 28, 2003

ABSTRACT: Although it is hypothesized that long-chain fatty acyl CoAs (LCFA-CoAs) and long-chain fatty acids (LCFAs) regulate transcription in the nucleus, little is known regarding factors that determine the distribution of these ligands to nuclei of living cells. Immunofluorescence colocalization showed that liver fatty acid-binding protein (L-FABP; binds LCFA-CoA as well as LCFA) significantly colocalized with PPARα in nuclei of transfected L-cell fibroblasts. Colocalization with a DNA binding dye (SYTO59) revealed that, within the nucleus of control L-cells, the nonhydrolyzable fluorescent LCFA-CoA (BODIPY-C16-S-S-CoA) was distributed primarily in a punctate pattern throughout the nucleoplasm, while nonmetabolizable fluorescent LCFAs (BODIPY-C16 and BODIPY-C12) were localized primarily near the nuclear envelope membranes. L-FABP overexpression selectively increased the targeting of BODIPY-C16-S-S-CoA by 1.9- and 2.7-fold into the nuclear membrane and nucleoplasm, respectively. L-FABP also increased the targeting of fluorescent LCFAs (especially long-chain-length BODIPY-C16) by 1.7-fold to the nuclear membrane and 7.4-fold into the nucleoplasm. A *cis*-parinaric acid displacement assay showed that L-FABP bound BODIPY-C12 and BODIPY-C16 with K_is of 10.1 ± 2.5 and 20.7 ± 1.5 nM, respectively, in the same range as naturally occurring LCFAs. Finally, solid-phase extraction and HPLC analysis revealed that, depending on the fatty acid content of the culture medium, L-FABP expression also increased the cellular LCFA-CoA pool size and altered the LCFA-CoA acyl chain composition. Thus, L-FABP may function as a carrier for selectively enhancing the distribution of LCFA-CoA, as well as LCFA, to nuclei for potential interaction with nuclear receptors.

Several recent discoveries suggest that long-chain fatty acyl CoAs (LCFA-CoA)[1] and long-chain fatty acids (LCFA) may be naturally occurring ligands for several nuclear receptors involved in regulating expression of multiple genes, especially those participating in lipid (PPARα, HNF4α, GR, TR, LXR, SREBP) and glucose (HNF4α) metabolism (reviewed in ref *1*). These lipid ligands interact with the ligand binding domains of the respective nuclear receptors, thereby eliciting conformational alterations which are thought to facilitate interaction with DNA, release of corepressors, or recruitment of coactivator complexes to regulate transcriptional activity (reviewed in ref *2*). Some nuclear receptors such as PPARα and HNF4α compete for binding to a number of promoters (*3*, *4*), suggesting the possibility of both synergistic or antagonistic cross-talk (depending on the specific LCFA-CoA or LCFA ligand) between PPARα and HNF4α (*5*).

Direct fluorescent binding assays demonstrated that PPARα has very high affinity (30 nM K_d) for a naturally occurring fluorescent LCFA (i.e., *trans*-parinaric acid) and even higher affinities (i.e., 5−17 nM K_ds) for other commonly occurring unsaturated [e.g., oleic acid (C18:1), linoleic acid (C18:2), linolenic acid (C18:3), arachidonic acid (C20:4)] but not saturated [stearic acid (C18:0), palmitic acid (C16:0)] LCFAs (*6*, *7*). Interestingly, other recent studies suggest that long-chain fatty acyl CoAs (LCFA-CoAs) may act as PPARα antagonists (*8*, *9*). *S*-Hexadecyl-CoA, a nonhydrolyzable palmitoyl-CoA analogue, antagonized the effects of agonists on PPARα conformation and function. The *S*-hexadecyl-CoA prevented ligand-induced interaction between the coactivators SRC-1 and PPARα but increased recruitment of the nuclear receptor corepressor NCoR (*9*).

Although HNF4α was originally recognized as an orphan nuclear receptor with no known ligand (reviewed in ref *5*) and structural models initially suggested no ligand binding site (*10*), recent studies established that HNF4α binds both long-chain fatty acyl CoAs (LCFA-CoAs) (*5*, *11*, *12*) and LCFAs (*11*−*14*) but with markedly different affinities. Direct fluorescent ligand binding and fluorescence resonance energy

† This work was supported in part by a grant from the USPHS National Institutes of Health (DK41402).

* To whom correspondence should be addressed. Phone: (979) 862-1433. Fax: (979) 862-4929. E-mail: fschroeder@cvm.tamu.edu.

‡ Department of Physiology and Pharmacology, Texas A&M University.

§ Oregon Graduate Institute of Science and Technology.

|| Department of Pathobiology, Texas A&M University.

[1] Abbreviations: HNF4α, hepatic nuclear factor 4α; LCFA-CoA, long-chain fatty acyl CoA; LCFA, long-chain fatty acid; L-FABP, liver fatty acid-binding protein; BODIPY, 4,4-difluoro-5,7-dimethyl-4-bora-3a,4a-diaza-*s*-indacene; LSCM, laser-scanning confocal microscopy; PPARα, peroxisome proliferator activated receptor α.

10.1021/bi0352318 CCC: $27.50
Published on Web 02/10/2004

transfer assays showed that HNF4α binds LCFA-CoAs (e.g., palmitoyl-, stearoyl-, linoleoyl-, and arachidonoyl-CoAs) with high affinity (i.e., 0.6−4.0 nM K_ds) (*11*, *12*). Interestingly, saturated LCFA-CoAs with chain lengths of 14 and 16 carbon atoms act as HNF4α agonists, whereas ω-3 and ω-6 polyunsaturated LCFA-CoAs and longer chain saturated LCFA-CoAs (C18:0-CoA) act as HNF4α antagonists (*5*, *12*). Consistent with the opposite effects of these ligands on transcription, the activating and inhibitory LCFA-CoAs oppositely affected HNF4α secondary structure as determined by circular dichroism (*11*). LCFA-CoAs are thought to modulate the transcriptional activity of HNF4α by either shifting the HNF4α oligomeric−dimeric equilibrium or affecting the intrinsic affinity of the HNF4α dimer for its cognate enhancer (*5*). Finally, HNF4α also binds naturally occurring LCFAs (arachidonic acid, *cis*-parinaric acid) as evidenced by direct binding assays showing K_ds ranging from 0.4 to 0.7 μM (*11*) and by X-ray crystallographic studies confirming the presence of bound LCFAs (*13*, *14*).

Despite the above important studies demonstrating that LCFA-CoAs and LCFAs bind to and are ligand activators of nuclear receptors, relatively little is known regarding factors that regulate the distribution of these ligands to the nucleus. One potential candidate protein that may serve in this capacity is the liver fatty acid-binding protein (L-FABP). Liver fatty acid-binding protein (L-FABP) is a highly abundant protein present in high concentration in the cytoplasm, 0.2−0.4 mM in liver, intestine, and kidney (reviewed in ref *15*). L-FABP binds both LCFAs and LCFA-CoAs (reviewed in refs *15*−*17*). Furthermore, a recent study suggested that L-FABP was involved in PPAR-regulated gene expression (*18*). A strict correlation was observed between PPARα and PPARγ transactivation with an intracellular concentration of L-FABP (*18*). However, it is not completely clear whether L-FABP transports bound ligands to the nucleus for interaction with PPARs. While a recent study suggests that L-FABP enhances the targeting of LCFAs to the nucleus of living cells, that report did not differentiate between LCFAs targeted to the nuclear envelope region vs the nucleoplasm within the nucleus (*19*). Finally, there have been no real-time studies demonstrating the presence of LCFA-CoAs in nuclei of living cells, the distribution of LCFA-CoAs in nucleoplasm and nuclear envelope membranes of living cells, or the potential role of L-FABP in targeting LCFA-CoAs to nuclei of living cells.

The objectives of the present investigation were to (i) determine if L-FABP and PPARα colocalize in nuclei of living L-FABP-expressing L-cells, (ii) utilize confocal fluorescence imaging, in conjunction with a nuclear marker, to show if L-FABP expression alters the distribution of fluorescent nonhydrolyzable LCFA-CoA and nonmetabolizable LCFA to nuclei of intact living cells, and (iii) resolve whether L-FABP expression alters the cellular LCFA-CoA pool size and LCFA-CoA acyl chain composition.

EXPERIMENTAL PROCEDURES

Materials. Nuclear DNA binding dyes (SYTO17, SYTO-59, SYTO60) and fluorescent fatty acid BODIPY-C12 and BODIPY-C16 (Figure 1) were purchased from Molecular Probes Inc. (Eugene, OR). BODIPY-C16-S-S-CoA (Figure 1) was custom synthesized by Molecular Probes Inc. according to a synthetic scheme developed by G. Woldegiorgis (*20*). Fetal bovine serum (FBS) and bovine serum albumin (BSA) were purchased from Sigma Chemical Co. (St. Louis, MO). Lab-Tek coverglass slides were purchased from Fisher Scientific (Pittsburgh, PA). The fatty acid composition of serum lipids was determined as described earlier (*21*). All reagents and solvents used were of the highest grade available and were cell culture tested as necessary.

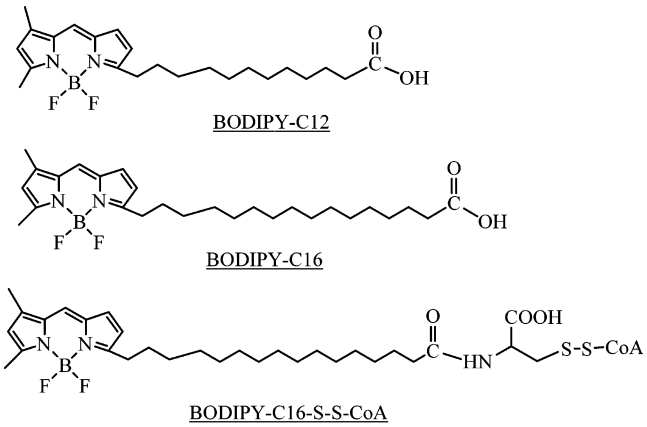

FIGURE 1: Chemical structures of BODIPY-C12, BODIPY-C16, and BODIPY-C16-S-S-CoA.

Antibodies. The primary antibodies used as markers for the nucleus were anti-LAP2 (Transduction Laboratories, BectonDickinson Biosciences, Lexington, KY), a marker for a protein present in the inner membrane of the nuclear envelope, and anti-C23 (Santa Cruz Biotechnologies Inc., Santa Cruz, CA), a marker for a nucleoli protein. The following anti-PPAR antibodies were purchased and tested with L-cell fibroblasts: rabbit polyclonal anti-all three isoforms (γ1 and γ2, 55−56 kDa; α, 52 kDa; β/δ/NUC1, 49 kDa) and monoclonal anti-PPARα from Affinity BioReagents (Golden, CO), goat polyclonal anti-PPARα from Santa Cruz Biotechnologies (Santa Cruz, CA), and rabbit polyclonal anti-all three isoforms (identical with the anti-PPARα from Affinity BioReagents) from Sigma (St. Louis, MO). All anti-PPAR antibodies were positive for cross-reaction with mouse antigens. Western blotting of L-cell homogenates with the above anti-PPAR antisera detected bands primarily near 52 kDa (PPARα) with smaller detectable bands near 56 kDa (PPARγ). Anti-L-FABP antibodies were obtained as previously described (*16*). The secondary antibodies used were alkaline phosphatase- (Sigma, St. Louis, MO) and HRP-conjugated antibodies (Pierce, Rockford, IL) for immunoblotting and FITC- (Sigma), Texas Red-, and Alexa-Fluor-conjugated antibodies (Molecular Probes, Eugene, OR) for immunofluorescence microscopy.

Cell Culture. Murine arpt$^-$ tk$^-$ (adenosine phosphoribosyl transferase deficient, thymidine kinase negative mutant) L-cell fibroblasts, mock-transfected control L-cells, and L-cells transfected with cDNA encoding for L-FABP (*22*) were grown in supplemented Higuchi medium (*23*).

Immunofluorescence Labeling. Cells were plated and grown on glass coverslips as well as chamber slides (Nalge Nunc International, Rochester, NY, or Fisher, Fair Lawn, NJ) (*19*). After removal of medium and washing three times with 75 mM phosphate buffer, pH 7.4, and 150 mM NaCl (PBS), cells were fixed and permeabilized by one of two

protocols: (i) 3.7% paraformaldehyde (Sigma, St. Louis, MO) and 1.5% methanol (Fisher, Fair Lawn, NJ), in PBS, pH 7.2 (GIBCO BRL, Grand Island, NY), 15 min; 1% Triton X-100 (Polysciences, Warrington, PA) in PBS, 5 min; extensive washing (five times in 30 min) with 0.1% Tween 20 (Fisher, Fair Lawn, NJ) in PBS; (ii) methanol, 20 °C, 5 min; 57 mM borate buffer, pH 8.2, for rehydration and subsequent steps. Autofluorescence of residual aldehyde groups was quenched with 100 mM NH_4Cl (Sigma, St. Louis, MO) in PBS. Nonspecific reactivity was blocked by using either 2% ovalbumin or BSA (Sigma, St. Louis, MO) in PBS or borate buffer, respectively. Incubations with primary antibodies diluted in 1% ovalbumin in buffer, as well as those with secondary antibodies (diluted in buffer only), in a humid chamber for 30 min at 37 °C, required subsequent extensive washing. For simultaneous colocalization experiments, mixtures of primary and secondary antibodies were used. Cover glasses were mounted on slides with SlowFade medium (Molecular Probes, Eugene, OR). Immunostaining specificity was established by using an indifferent antibody, omitting the primary antibody, and using either one or both of the secondary antibodies, which allowed minimization of nonspecific absorption of fluorescent antibodies (background), optimal separation of the fluorophore fluorescent signals, and optimization of fluorophore concentration to preclude self-quenching.

Fluorescence Emission Spectra of BODIPY-C12 in the Presence and Absence of L-FABP. BODIPY-C12 stock solutions were prepared in 10 mM NaOH to produce the sodium salt to minimize formation of fluorescent micelles. BODIPY-C12 was diluted to 0.7 nM in PBS, and its fluorescence emission spectrum was recorded with an ISS PC1 photon counting fluorometer (ISS Instruments Inc., Champaign, IL) at 24 °C with a circulating water bath. The emission spectrum was measured from 490 to 560 nm while the excitation wavelength was set at 460 nm. Then BODIPY-C12 was incubated with L-FABP (0.18 μM) for 5 min to obtain maximum binding before its emission spectrum was recorded again under the same conditions.

L-FABP Fluorescence Ligand Binding Assay: Displacement of L-FABP-Bound cis-Parinaric Acid by BODIPY-C12 and BODIPY-C16. L-FABP binding of fluorescent ligands (BODIPY-C12 and BODIPY-C16) was performed by a displacement assay basically as described earlier (*16*). Briefly, L-FABP (0.18 μM) in PBS was incubated with *cis*-parinaric acid (0.15 μM) for 5 min at 24 °C to obtain maximal fluorescence. L-FABP-bound *cis*-parinaric acid was displaced with an increasing amount of BODIPY-C12 (0−133 nM) or BODIPY-C16 (0−177 nM). *cis*-Parinaric acid emission spectra were obtained with an ISS PC1 photon counting fluorometer (ISS Instruments Inc., Champaign, IL) with excitation at 318 nm and emission from 375 to 490 nm. To avoid formation of micelles, BODIPY-C12 and BODIPY-C16 were used as their sodium salts prepared by dissolving free fatty acids in 10 mM NaOH. The sample temperature was maintained at 24 °C using a circulating water bath.

The displacement binding curves were constructed by plotting *cis*-parinaric acid fluorescence intensity at the emission maximum (411 nm) vs BODIPY-C12 or BODIPY-C16 concentration. The concentration $[I_{50}]$ of BODIPY LCFA at 50% displacement was obtained from the curve fitting using SigmaPlot software. The K_i of BODIPY LCFA displacing *cis*-parinaric acid was calculated using the equation (*24*):

$$K_i = [I_{50}]/(1 + [L]/K_L)$$

where $[L] = 0.15$ μM is the concentration of *cis*-parinaric acid and $K_L = 171 \pm 46$ nM (*16*) is the dissociation constant of *cis*-parinaric acid binding to L-FABP.

Fluorescence Spectra of BODIPY-C16-S-S-CoA and SYTO-59−DNA. Fluorescence excitation and emission spectra of BODIPY-C16-S-S-CoA and SYTO59−DNA were obtained with an ISS PC1 photon counting fluorometer (ISS Instruments Inc., Champaign, IL). Spectra were recorded in ethanol at 24 °C with a circulating water bath. The spectra were recorded as follows: excitation spectrum of BODIPY-C16-S-S-CoA, $\lambda_{ex} = 400-520$ nm, $\lambda_{em} = 530$ nm; emission spectrum of BODIPY-C16-S-S-CoA, $\lambda_{ex} = 465$ nm, $\lambda_{em} =$ 495 to 650 nm; excitation spectrum of the SYTO59−DNA complex, $\lambda_{ex} = 465-630$ nm, $\lambda_{em} = 640$ nm; emission spectrum of the SYTO59−DNA complex, $\lambda_{ex} = 570$ nm, $\lambda_{em} = 600-800$ nm. The spectra obtained were normalized.

Vital Staining with SYTO59 and Fluorescent LCFA-CoA (BODIPY-C16-S-S-CoA) or Fluorescent LCFAs (BODIPY-C16, BODIPY-C12) for Real-Time Laser Scanning Confocal Microscopy (LSCM) in Living Cells. Cell cultural media were removed, and the cells were washed with PBS (two times). Control L-cells and L-FABP-expressing cells were incubated with a DNA binding dye SYTO59 (final concentration 1.25 μM) for 30 min in PBS at room temperature. Background images were then taken, followed by addition of BODIPY-C16-S-S-CoA, BODIPY-C16, or BODIPY-C12 (final concentration 0.1 μM) and immediate acquisition of successive images every 20 s over the next 30 min.

Image Acquisition by Laser Scanning Confocal Microscopy (LSCM). LSCM images were acquired with an Axiovert 135 microscope (Zeiss; Carl Zeiss Inc., Thornwood, NY) and MRC-1024 LSCM fluorescence imaging system (Bio-Rad, Hercules, CA) as described previously (*19*). The BODIPY and SYTO59 probes were excited with laser 488/568 lines. The images of BODIPY fluorescence were collected with a 522/D35 emission filter in mixer A, while the images of SYTO59−DNA/RNA were collected with an 680/32 emission filter in mixer B, both under manual gain and black level control. The objective was focused to acquire 0.3 μm confocal slice images through a median section of cells in the field. Images were collected every 20 s. Cells were excited for 0.1 s intervals, regulated by a computer-controlled shutter and LaserSharp software (Bio-Rad Inc., Hercules, CA).

Analysis of Laser Scanning Confocal Microscopy (LSCM) Images. Images were analyzed using LaserSharp (Bio-Rad Inc., Hercules, CA) and MetaMorph Image Analysis (Advanced Scientific Imaging, Meraux, LA) software. The fluorescence intensity of the medium was set to zero, and increase above zero was recorded as arbitrary units (au). Autofluorescence was very low at the level of background. Fluorescent intensity in images of single living cells was expressed as the mean fluorescence intensity in gray scale units expressed ±SE. The regions of interest measured were the nucleoplasm, the nuclear membrane, and the cytoplasm (including all other intracellular membranes). Images of

fluorescent BODIPY-C16-S-S-CoA, BODIPY-C16, or BODIPY-C12 were used to plot the increase in intensity over time. Linear regression analysis was used to define the linear portion of the uptake curves and to obtain the initial uptake rate. Statistical analysis was performed using Student's *t*-test.

Solid-Phase Extraction of Long-Chain Fatty Acyl CoA from Cultured Cells. Cells harvested from the culture dish (100 × 20 mm) were suspended in 100 mM KH_2PO_4 with protease inhibitor, pH = 5.3 (1 mL). After addition of the internal standard, heptadecanoyl CoA (C17:0-CoA, 10 pmol), the samples were processed and LCFA-CoAs were extracted from control and L-FABP-expressing L-cell fibroblasts using a solid-phase extraction procedure (*25*, *26*).

Formation of Fluorescent Long-Chain Fatty Acyl Etheno CoA Derivatives and Reversed-Phase HPLC Separation and Quantitative Analysis of Long-Chain Fatty Acyl Etheno CoA Ester Mixtures. Fluorescent long-chain fatty acyl etheno CoA derivatives were formed by reaction of LCFA-CoA standards and liver LCFA-CoA extracts with chloroacetaldehyde reagent as described previously (*25*, *27*). Long-chain fatty acyl etheno CoA derivatives were separated and quantitated using the reverse-phase HPLC method (*25*) developed on the basis of an earlier report (*27*). The peaks were identified by comparing the retention times with those of etheno-LCFA-CoAs formed from known LCFA-CoA standards, and the quantitation of each unknown was performed by calculation of relative peak areas to that of a known amount of the internal standard etheno-C17:0-CoA.

Calculation of Ligand and L-FABP Concentrations in L-Cell Nuclei and Cytoplasm (plus Plasma Membrane). L-FABP-expressing and control L-cells were incubated with BODIPY-C12, BODIPY-C16, or BODIPY-C16-S-S-CoA (final concentration 0.1 μM) for 30 min. Quantitative chemical analysis showed that the total uptake of BODIPY-C12 and BODIPY-C16 by L-cells was 0.29 ± 0.03 and 0.68 ± 0.08 nmol/mg of protein, respectively (*19*). The amount of BODIPY-C16-S-S-CoA inside the cells was estimated from its fluorescence intensity compared with that of BODIPY-C12 under the same experimental conditions. The amount of BODIPY-C12, BODIPY-C16, and BODIPY-C16-S-S-CoA in different cellular compartments was estimated by the percent distribution (determined by LSCM fluorescence imaging) in nuclei and in the cytoplasm (plus plasma membrane) from the medial cross-sectional plane (see Results, Figure 8), based on which the percent distribution in the whole nucleus and cytoplasm (plus plasma membrane) was calculated. The cellular protein concentration was 12.4 ± 1.0 $\mu g/10^6$ cells. The L-cell fibroblast volume was estimated to be 7 pL per cell on the basis of previous determinations for fibroblasts (*28*). The volume of the nucleus was estimated to be about 23% of the cell volume (*29*). The fold increase in total uptake for L-FABP-expressing L-cells compared with control L-cells was obtained as indicated in the Results section (see Table 1). Final concentrations were calculated from the amount of BODIPY-C12, BODIPY-C16, and BODIPY-C16-S-S-CoA in the nucleus and in the cytoplasm (plus plasma membrane) divided by the estimated respective volumes of the nucleus and the cytoplasm (plus plasma membrane).

The concentrations of L-FABP in nuclei and the cytoplasm (plus plasma membrane) of L-FABP-expressing and control (mock-transfected) L-cells were calculated from the amount of L-FABP in the nucleus and in the cytoplasm divided by the estimated volume of the nucleus and the cytoplasm, respectively, as described above. L-FABP accounts for 0.4% of all soluble proteins of L-FABP-expressing L-cells (*30*, *31*) determined by western blot. The percentage of L-FABP in the nucleus and in the cytoplasm was estimated from the L-FABP immunofluorescent image of L-FABP-expressing L-cells (see Results, Figure 1A).

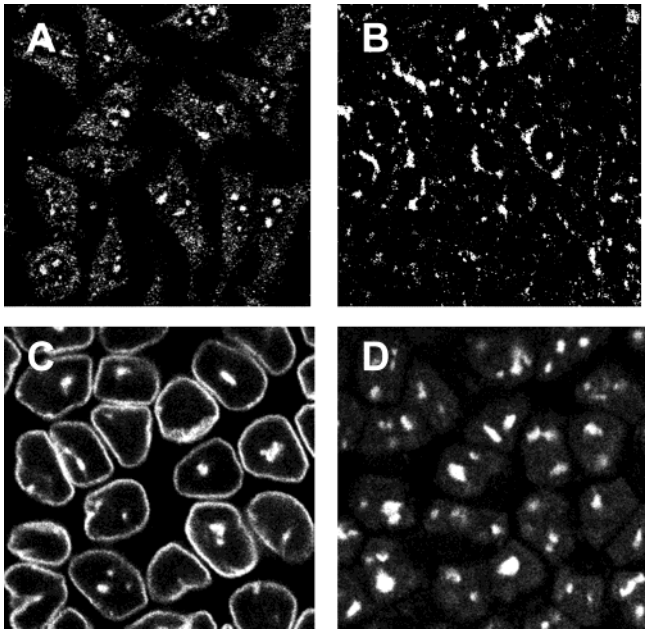

FIGURE 2: Immunofluorescence localization of L-FABP (panel A), PPARα (panel B), LAP2 (panel C), and C23 (panel D) in L-FABP-expressing L-cells. L-FABP-expressing cells were fixed, permeabilized, and incubated with primary antibodies (polyclonal rabbit anti-L-FABP, polyclonal rabbit anti-PPARα, monoclonal anti-LAP2, and monoclonal anti-C23, respectively), followed by secondary antibodies (FITC-conjugated goat anti-rabbit IgG), and images were obtained by laser scanning confocal microscopy as described in Experimental Procedures. The fluorescence image in panel A revealed that most of the L-FABP was diffusely distributed in the cytoplasm and a lesser amount of L-FABP was distributed in a punctate pattern within nuclei. Panel B showed PPARα was concentrated within nuclei as groups of dots and near the nuclear envelope. Panel C showed the contour of the nuclear envelope highlighted by labeling with the anti-LAP2 antibody, a marker for the inner membrane of the nuclear envelope. In addition, a bright spot or circle of anti-LAP2 immunoreactivity was detected at the middle of some nuclei, consistent with invaginations of the nuclear envelope. Panel D showed that multiple nucleoli in different sizes and shapes were present in most cells, well restricted to the nuclei.

RESULTS

Immunofluorescence Localization of L-FABP in L-FABP-Expressing L-Cell Fibroblasts. LSCM fluorescence images revealed that L-FABP was detectable in a speckled pattern throughout the cell with a denser group in the middle, presumably within the nucleus whose demarcation was not clearly discernible (Figure 2A). The speckled appearance of L-FABP in the cytoplasm may represent the diffuse, soluble L-FABP and some L-FABP associated with membranes (endoplasmic reticulum, mitochondria) as has previously been demonstrated for rat liver (*32*). Finally, this pattern of L-FABP distribution in L-FABP-expressing L-cells was similar to that observed in liver hepatocytes and embryonic stem cells (*32*, *33*). Quantitative analysis of the images

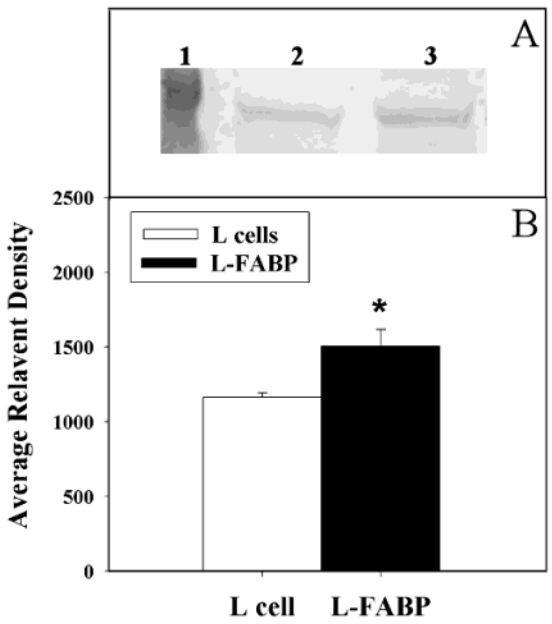

FIGURE 3: Western blotting of PPARα in control and L-FABP-expressing cells. Panel A: representative western blot of homogenates from control mock-transfected L-cells (lane 2) and L-FABP-expressing L-cells (lane 3). Lane 1 contains a molecular weight standard. Panel B: densitometric analysis of multiple western blots to determine the relative amount of PPARα in control mock-transfected L-cells and L-FABP-expressing L-cells. An asterisk refers to $p < 0.05$, $n = 3$.

revealed that 19.5 ± 1.0% of the anti-L-FABP immunofluorescence intensity was in nuclei while 78.1 ± 2.3% was in the cytoplasm. The concentrations of L-FABP in nuclei and the cytoplasm were calculated to be 43.2 ± 2.2 and 51.4 ± 1.5 μM, respectively. Thus, the high concentration of L-FABP in bright punctate areas within nuclei resulted in L-FABP concentrations being nearly equivalent in nuclei and cytoplasm.

Immunofluorescence Localization of PPARα in Nuclei of L-FABP-Expressing L-Cell Fibroblasts. Although PPARα is found in highest levels in liver hepatocytes, western blotting of homogenates from control (mock-transfected) and L-FABP-expressing L-cell fibroblasts detected PPARα (Figure 3A). Quantitative comparison of multiple western blots revealed that L-FABP expression increased the level of PPARα by 29% ($p < 0.03$, $n = 3$) (Figure 3B). Immunofluorescence LSCM images showed PPARα appeared to be concentrated within nuclei as groups of dots, occasionally near the nuclear envelope (Figure 2B). A small amount of diffuse and punctate labeling also occurred in the cytoplasm of some cells. These data indicated that the highest level of PPARα was detected in the nuclei. The following experiments were performed to further discriminate (i) whether PPARα near the nuclear envelope was perinuclear in the cytoplasm or within the nucleus and (ii) whether PPARα punctate labeling in the nucleoplasm was associated with nucleoli.

When transfected L-cells expressing L-FABP were labeled with anti-LAP2, a marker for the inner membrane of the nuclear envelope, the contour of the nuclear envelope was distinctly highlighted (Figure 2C). A bright spot or circle of anti-LAP2 immunoreactivity was detected at the middle of some nuclei, consistent with invaginations of the nuclear envelope. Colocalization of PPARα with LAP2 was achieved by double immunolabeling. Simultaneously acquired LSCM images were superimposed to yield a merged image (Figure 4A). PPARα colocalized with LAP2 appeared as yellow pixels in Figure 4A, indicating that PPARα near the nuclear envelope was associated with the inner nuclear membrane. After background subtraction, the colocalization coefficients were calculated to be red (PPARα), 0.44 ± 0.02 (mean ± SE, $n = 21$), and green (LAP2), 0.14 ± 0.01 (mean ± SE, $n = 21$). Therefore, on the middle cross-sectional plane, approximately 44% of PPARα was colocalized with LAP2 at the nuclear inner membrane.

Next, L-FABP-expressing cells were labeled with anti-C23, a marker for nucleoli. The images showed that multiple nucleoli were present in most cells as very distinct globular structures, well restricted to the nuclei (Figure 2D). The nucleoli were not only present in multiple numbers per nucleus but also appear in different sizes and shapes. It must be noted that, although it is possible that the anti-C23 antibody also stains cytoplasmatic phosphorylated nucleolin, in L-cells apparently only the nuclear unphosphorylated form was present. Cells were then double immunolabeled with polyclonal rabbit anti-PPARα and monoclonal anti-C23, images being simultaneously acquired, and superimposed to yield a merged image to determine colocalization (Figure 4B). PPARα colocalized with C23 appeared as yellow punctate structures in Figure 4B. Some punctate PPARα within the nucleoplasm colocalized within the nucleoli, as indicated by partial overlap (yellow pixels) of the anti-PPARα immunoreactivity with dotted areas specific for nucleolin (C23) (Figure 4B). After background subtraction, the colocalization coefficients were calculated to be red (PPARα), 0.45 ± 0.06 (mean ± SE, $n = 18$), and green (C23), 0.46 ± 0.04 (mean ± SE, $n = 18$). Therefore, in the middle cross-sectional plane, approximately 45% of PPARα was colocalized with nucleoli marker C23.

In summary, PPARα was distributed primarily within the nucleus, most intensely near the inner nuclear membrane (determined with anti-LAP2) and in nucleoli (determined with anti-C23). Low levels of PPARα were distributed diffusely within the nucleoplasm. A small amount of diffuse and punctate PPARα labeling was also detected in the cytoplasm of some cells.

Immunofluorescence Colocalization of PPARα and L-FABP in L-FABP-Expressing L-Cell Fibroblasts. To determine if PPARα in the nucleus colocalized with L-FABP in L-FABP-expressing L-cells, the cells were double immunolabeled with anti-PPARα and anti-L-FABP, followed by LSCM. Simultaneously acquired images were superimposed to yield a merged image wherein colocalized PPARα and L-FABP in the nuclei appeared as yellow punctate structures (Figure 4C). L-FABP colocalized with PPARα primarily in areas close to the nuclear envelope and also as bright spots in the nucleoplasm (Figure 4C). Some L-FABP also colocalized with PPARα diffusely in the nucleoplasm. After background subtraction, the yellow pixels illustrating that PPARα colocalized with L-FABP were shown in Figure 4D. The colocalization coefficients of red (PPARα) and green (L-FABP) pixels were calculated to be red, 0.30 ± 0.02 (mean ± SE, $n = 13$), and green, 0.23 ± 0.02 (mean ± SE, $n = 13$). Therefore, on the middle cross-sectional plane, approximately 30% of PPARα was colocalized with L-

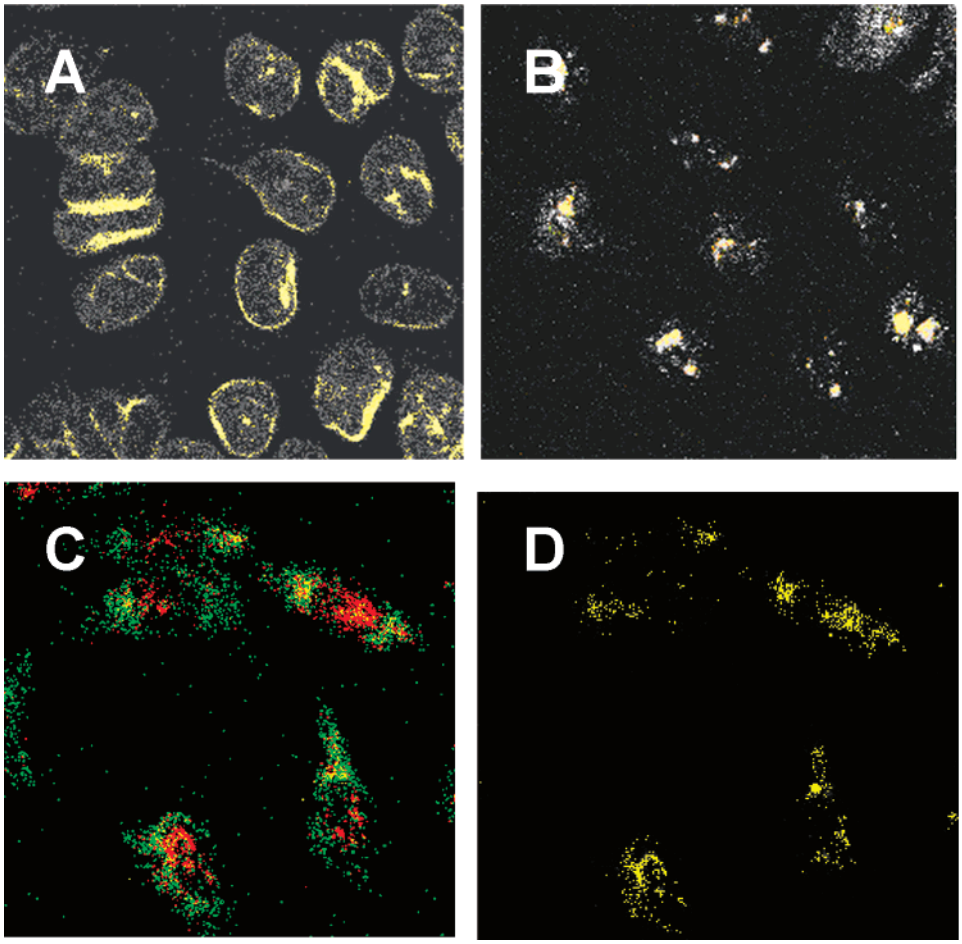

FIGURE 4: Colocalization of PPARα with nuclear markers and L-FABP in L-FABP-expressing L-cells. Double immunolabeling with polyclonal rabbit anti-PPARα and monoclonal anti-LAP2 (panel A), monoclonal anti-C23 (panel B), or polyclonal rat anti-L-FABP (panel C) and laser scanning confocal microscopy were performed as described in Experimental Procedures. Simultaneously acquired images were superimposed to yield a merged image. Colocalized PPARα and LAP2, C23, or L-FABP, respectively, appeared as yellow punctate structures. PPARα was distributed primarily within the nucleus, most intensely near the inner nuclear membrane (determined with anti-LAP2, panel A) and in nucleoli (determined with anti-C23, panel B). Small levels of PPARα were distributed diffusely within the nucleoplasm. L-FABP colocalized with PPARα primarily in areas close to the nuclear envelope and also as bright spots in the nucleoplasm. Some L-FABP also colocalized with PPARα diffusely in the nucleoplasm (panels C and D).

FABP, and about 23% of the L-FABP was colocalized with PPARα.

Effect of Binding to L-FABP on BODIPY-C12 Fluorescence. Since the quantum yield of many fluorescent molecules is enhanced when protein bound, this could complicate interpretation of enhanced cellular and nuclear BODIPY fluorescence in L-FABP-expressing cells. To address this issue, the fluorescence intensity of BODIPY-C12 was determined in solution with and without L-FABP. As shown in Figure 5A, upon binding to L-FABP, BODIPY-C12 fluorescence did not increase (dotted line). Instead, the BODIPY-C12 emission spectrum maximum shifted from 514 to 520 nm, and the fluorescence intensity decreased slightly. Thus, the increased fluorescence of BODIPY fatty acids upon cellular uptake (measured at 530 nm) was not due to enhanced intensity upon protein binding.

Affinity of L-FABP for BODIPY-C12 and BODIPY-C16. The affinity of L-FABP for BODIPY fatty acids was measured through a fluorescence displacement assay utilizing *cis*-parinaric acid, a naturally occurring fluorescent fatty acid, as previously described for L-FABP (*16*) and nuclear receptors (*6*). *cis*-Parinaric acid is not fluorescent in PBS buffer solution, but upon binding to L-FABP the fluorescence intensity of *cis*-parinaric acid increases. If BODIPY-C12 and BODIPY-C16 compete with *cis*-parinaric acid for the L-FABP binding site to displace *cis*-parinaric acid, the *cis*-parinaric acid would be released back to the aqueous environment and its fluorescence intensity is expected to decrease. As expected, the fluorescence intensity of *cis*-parinaric acid bound to L-FABP decreased with increasing amounts of BODIPY-C12 (Figure 5B) and BODIPY-C16 (Figure 5D), respectively. From the displacement binding curves of BODIPY-C12 (Figure 5C) and BODIPY-C16 (Figure 5E), the K_is were calculated to be 10.1 ± 2.5 and 20.7 ± 1.5 nM, respectively. Thus, the affinities of L-FABP for BODIPY-C12 and BODIPY-C16 were in the same range as the affinity of L-FABP for naturally occurring fatty acids (*16*).

BODIPY-C16-S-S-CoA Was Nonhydrolyzable. To establish whether BODIPY-C16-S-S-CoA was nonhydrolyzable under the conditions of the assay, L-cell fibroblasts were incubated for up to 30 min with Higuchi medium containing varying concentrations of BODIPY-C16-S-S-CoA. At the end of the incubation, cells were washed, LCFA-CoAs were extracted by solid-phase extraction, and the LCFA-CoAs were then analyzed by HPLC (*26*). Incubation of cells with BODIPY-

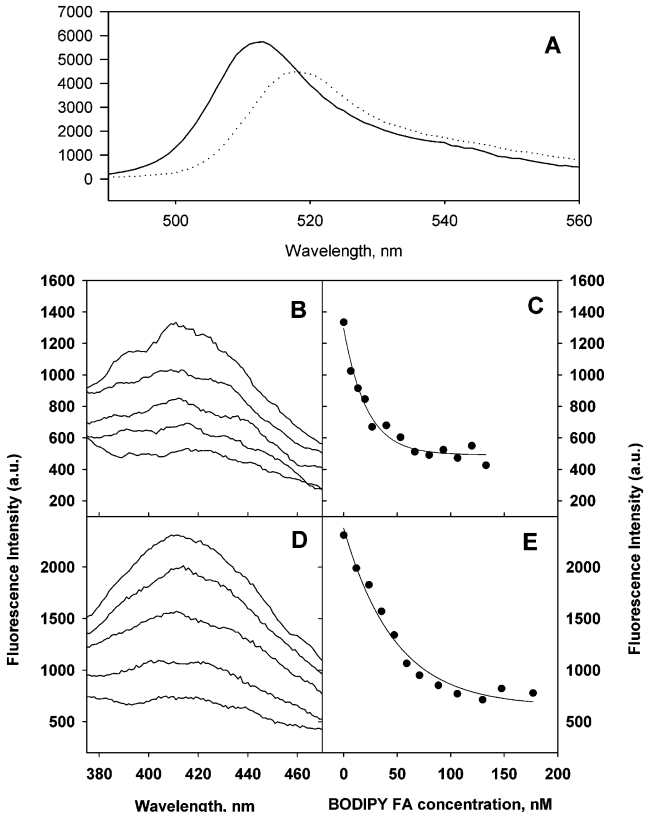

FIGURE 5: Displacement of L-FABP-bound *cis*-parinaric acid by BODIPY-C12 and BODIPY-C16. BODIPY-C12 (0.7 nM) fluorescence emission spectra (panel A, $\lambda_{ex} = 460$ nm and $\lambda_{em} = 490-560$ nm) in the presence (dotted line) and absence (solid line) of L-FABP (0.18 μM) showed, upon binding to L-FABP, that the BODIPY-C12 fluorescence emission maximum shifted to longer wavelength with decreased intensity. L-FABP-bound *cis*-parinaric fluorescence emission spectra (L-FABP, 0.18 μM; *cis*-PA, 0.15 μM; $\lambda_{ex} = 318$ nm, $\lambda_{em} = 375-470$ nm) in the presence of increasing amounts of BODIPY-C12 and BODIPY-C16 are shown in panels B and D. Panel B, from top to bottom BODIPY-C12 concentration: 0, 6.7, 20.0, 26.6, and 66.5 nM. Panel D, from top to bottom BODIPY-C16 concentration: 0, 12.0, 36.0, 60.0, and 132.0 nM. Panels C and E show the binding curves of BODIPY-C12 (0−133 nM) and BODIPY-C16 (0−177 nM) displacing L-FABP-bound *cis*-parinaric acid (L-FABP, 0.18 μM; *cis*-PA, 0.15 μM; $\lambda_{ex} = 318$ nm, $\lambda_{em} = 411$ nm).

C16-S-S-CoA for up to 30 min did not significantly alter the content of BODIPY-C16-S-S-CoA detected. Thus, like other types of LCFA-CoA analogues [e.g., *S*-hexadecyl-CoA, *S*-(2-oxo)pentadecyl-CoA, heptadecan-2-onyldethio-CoA] (*8*, *34*−*36*), BODIPY-C16-S-S-CoA was nonhydrolyzable.

Development of a Nuclear Marker for Determining the Distribution of Fluorescent Long-Chain Fatty Acids (BODIPY-C12 and BODIPY-C16) and Acyl CoA (BODIPY-C16-S-S-CoA) to the Nucleus of L-Cell Fibroblasts: SYTO Dyes.

The distribution of several SYTO nucleic acid stains was examined in L-cells. Of the SYTO dyes tested (SYTO17, SYTO59, and SYTO60), SYTO59 was optimal for L-cells. SYTO59 uptake reached a maximum before 30 min for both control L-cells and L-FABP-expressing L-cells (not shown). SYTO59 became highly fluorescent upon binding to nucleic acids and essentially exclusively labeled nuclear DNA in both control (mock-transfected) L-cells (Figure 7B) and L-FABP-expressing L-cells (Figure 7D). There was no significant difference in SYTO59 uptake between the L-FABP-expressing cells and control L-cells. Control experiments (not shown) were also performed to show that SYTO59 uptake did not interfere with BODIPY-labeled LCFA and LCFA-CoA uptake into the cell or into nuclei.

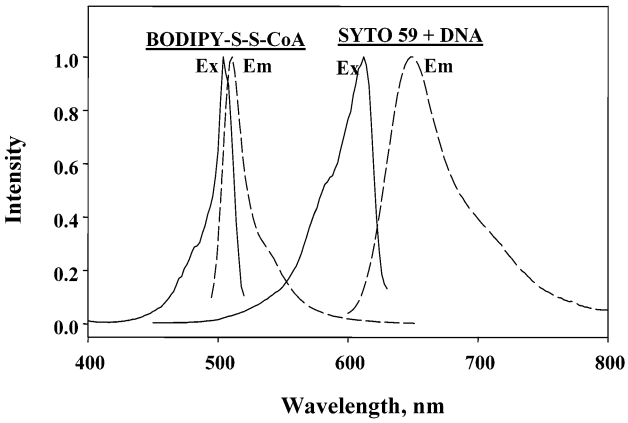

FIGURE 6: Spectral properties of BODIPY-C16-S-S-CoA and SYTO59−DNA. Excitation and emission spectra were obtained with an ISS PC1 photon counting fluorometer as described in Experimental Procedures. The excitation spectrum of BODIPY-C16-S-S-CoA was recorded from 400 to 520 nm while the emission was set at 530 nm. The emission spectrum of BODIPY-C16-S-S-CoA was recorded from 495 to 650 nm while the molecule was excited at 465 nm. The excitation spectrum of SYTO59−DNA was recorded from 465 to 630 nm while the emission was set at 640 nm. The emission spectrum of SYTO59−DNA was recorded from 600 to 800 nm while the molecule was excited at 570 nm.

The spectra of the SYTO59−nucleic acid complex showed an excitation maximum wavelength at 610 nm and emission maximum wavelength at 635 nm (Figure 6). Since BODIPY-labeled LCFAs and BODIPY-C16-S-S-CoA have excitation wavelengths at 505 nm and emission wavelengths at 510 nm (Figure 6), the emissions of BODIPY and SYTO59 were distinct. When both SYTO59 and BODIPY were excited with a 488/568 nm laser, BODIPY emission was independently monitored through a 522/D35 cutoff filter. The iris and gain were adjusted so there was no signal leakage between the two channels.

In summary, as shown in Figure 7B,D, SYTO59 stained the nuclei very precisely, with essentially no detectable SYTO59 outside the nucleus. BODIPY and SYTO59 fluorescence emissions were distinct and did not overlap. These characteristics were therefore utilized to quantitate the distribution of BODIPY-labeled LCFAs and LCFA-CoAs into the nucleus and to determine the effect of L-FABP expression on this distribution in the following sections.

Real-Time Determination of Fluorescent Fatty Acid (BODIPY-C12, BODIPY-C16) and Fluorescent Fatty Acyl CoA (BODIPY-C16-S-S-CoA) Uptake and Distribution to the Nucleus of Living L-Cell Fibroblasts: Effect of L-FABP Expression. To determine if expression of L-FABP enhanced the uptake and/or increased the distribution of long-chain fatty acid to the nucleus, laser scanning confocal microscopy was used to monitor the uptake of fluorescent LCFA (BODIPY-C12, BODIPY-C16) and fluorescent LCFA-CoA (BODIPY-C16-S-S-CoA) molecules as a function of time.

The fluorescent, medium-chain-length BODIPY-C12 was readily taken up by both control L-cells (Figure 7A) and L-FABP-expressing cells (Figure 7C), shown after 15 min incubation. In control (mock-transfected) L-cells the BODIPY-C12 was primarily distributed in the cytoplasm, with only small amounts in the dark nucleus (Figure 7A),

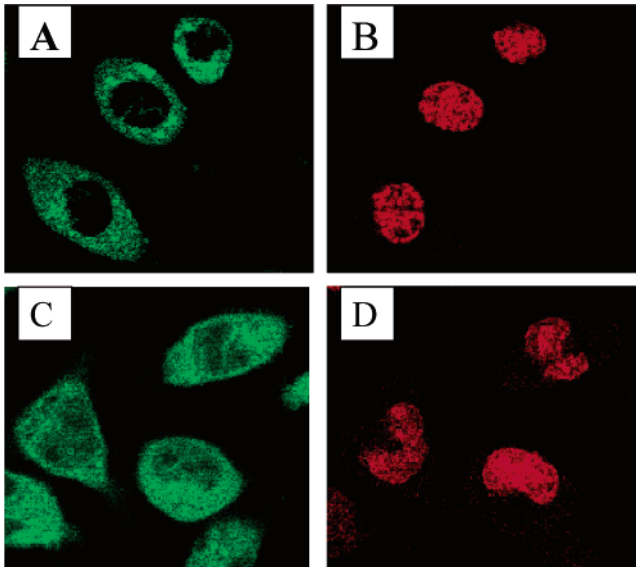

FIGURE 7: Laser scanning confocal microscopy of BODIPY-C12 (panel A, control L-cells; panel C, L-FABP-expressing cells) and SYTO59 (panel B, control L-cells; panel D, L-FABP-expressing cells). Control L-cells and L-FABP-expressing cells were incubated with SYTO59 (final concentration 1.25 μM) for 30 min in PBS at room temperature, BODIPY-C12 (final concentration 0.1 μM) was added to the media, and 15 min later the images were taken. The probes were excited with laser 488/568 lines. The signals from BODIPY-C12 were collected in mixer A with a 522/D35 emission filter, while the signals of SYTO59−DNA/RNA were collected in mixer B with a 680/32 emission filter. SYTO59 became highly fluorescent upon binding to nucleic acids and essentially exclusively labeled nuclear DNA in both control (mock-transfected) L-cells (panel B) and L-FABP-expressing L-cells (panel D). In control (mock-transfected) L-cells the BODIPY-C12 was primarily distributed in the cytoplasm, with only small amounts in the dark nucleus (panel A). In contrast, in L-FABP-expressing cells BODIPY-C12 emission was more intense, and much more BODIPY-C12 localized in the dark nuclear region (panel C).

appearing as solid red with simultaneously acquired images of SYTO59 in the same cells (Figure 7B). When the simultaneously acquired BODIPY-C12 (green) and SYTO59 (red) images in control L-cells were superimposed, colocalized pixels were detected as yellow pixels. When only colocalized (yellow) pixels displayed, it was apparent that BODIPY-C12 colocalized with the DNA binding dye (SYTO59) primarily near the edge of DNA staining (i.e., nuclear envelope) with smaller amounts distributed within the nucleoplasm (Figure 8A) of control L-cells. The colocalization coefficiencies were calculated to be red, 0.27 ± 0.02 (mean ± SE, $n = 12$), and green, 0.10 ± 0.01 (mean ± SE, $n = 12$). This suggested that, in the middle cross-sectional plane of control L-cells, 10% of the BODIPY-C12 (medium-chain-length fatty acid) was colocalized with SYTO59 in nuclei. Basically, control L-cells exhibited the same pattern of distribution for the longer chain BODIPY-C16 colocalizing with SYTO59 (Figure 8C). The colocalization coefficiencies were red, 0.13 ± 0.02 (mean ± SE, $n = 11$), and green, 0.17 ± 0.02 (mean ± SE, $n = 11$), which indicated that, in the cross-sectional plane of control L-cells, 17% of the BODIPY-C16 (long-chain-length fatty acid) was colocalized with SYTO59 in nuclei. The qualitative distribution pattern of both these BODIPY-labeled LCFAs in L-FABP-expressing cells differed markedly from that in control L-cells. BODIPY-C12 (Figure 7C) emission was more intense, and much more BODIPY-C12 was localized

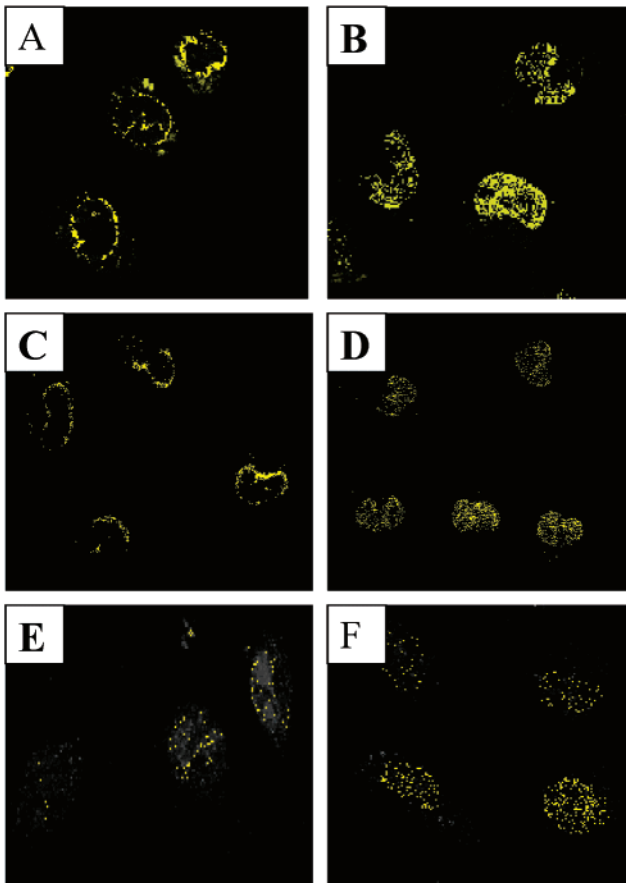

FIGURE 8: Colocalization of fluorescent fatty acids (BODIPY-C12, BODIPY-C16) and fatty acyl CoA (BODIPY-C16-S-S-CoA) with SYTO59 by laser scanning confocal microscopy. Representative images are shown after 15 min incubation of cells with the respective ligands as described in Experimental Procedures and in the legend for Figure 4. When the simultaneously acquired BODIPY (green) and SYTO59 (red) images were superimposed, colocalized pixels were detected as yellow pixels. The yellow pixels shown are when the green and red pixels were removed. It was apparent that in control L-cells BODIPY-C12 (panel A) and BODIPY-C16 (panel C) colocalized with SYTO59 primarily near the nuclear envelope with smaller amounts distributed within the nucleoplasm. In L-FABP-expressing cells much more BODIPY-C12 (panel B) and BODIPY-C16 (panel D) colocalized with SYTO59 not just near the nuclear envelope but with large amounts distributed throughout the nucleoplasm. In control L-cells, BODIPY-C16-S-S-CoA and SYTO59 colocalized pixels were diffusely and bright-punctuate distributed throughout the nucleoplasm (panel E). In L-FABP-expressing cells the distribution of BODIPY-C16-S-S-CoA colocalized with SYTO59 was brighter, but with similar diffusely and bright-punctuate distributed throughout the nucleoplasm (panel F).

in the dark nuclear region (Figure 7C), appearing as solid red with SYTO59 (Figure 7D). This was even more apparent when the simultaneously acquired BODIPY-C12 and SYTO-59 images in L-FABP-expressing L-cells were superimposed and only colocalized (yellow) pixels displayed (Figure 8B). In L-FABP-expressing cells much more BODIPY-C12 colocalized with the DNA binding dye (SYTO59) not just near the edge of DNA staining (i.e., nuclear envelope) but with large amounts distributed throughout the nucleoplasm (Figure 8B). The colocalization coefficiencies were calculated to be red, 0.89 ± 0.04 (mean ± SE, $n = 15$), and green, 0.26 ± 0.03 (mean ± SE, $n = 15$). This suggested that, in the cross-sectional plane of L-FABP-expressing L-cells, 26% of the BODIPY-C12 was colocalized with SYTO59 in nuclei,

severalfold higher than in control cells. In L-FABP-expressing cells the colocalization coefficiencies for the longer chain BODIPY-C16 (Figure 8D) were red, 0.36 ± 0.08 (mean ± SE, $n = 7$), and green, 0.28 ± 0.02 (mean ± SE, $n = 7$), indicating that in the cross-sectional plane of L-FABP-expressing L-cells 28% of the BODIPY-C16 was colocalized with SYTO59 in nuclei, severalfold higher than in control cells.

To determine if L-FABP expression also affected the qualitative distribution of the nonhydrolyzable BODIPY-C16-S-S-CoA within the cell, the above experiments were repeated except that BODIPY-C16-S-S-CoA uptake was examined. Since colocalization of BODIPY-C16-S-S-CoA green pixels with the SYTO59 red pixels yields yellow colocalized pixels, only the yellow colocalized pixels are shown in Figure 8E. BODIPY-C16-S-S-CoA significantly colocalized with SYTO59 in control L-cells. The colocalization coefficiencies were red, 0.027 ± 0.006 (mean ± SE, $n = 7$), and green, 0.09 ± 0.02 (mean ± SE, $n = 7$), which meant that, on the cross-sectional plane of control L-cells, 9% of the BODIPY-C16-S-S-CoA was colocalized with SYTO59 in the nucleus. It is important to note that, in control L-cells, the pattern of the fluorescent LCFA-CoA (i.e., BODIPY-C16-S-S-CoA) colocalization with the DNA binding dye SYTO59 in the nucleus (Figure 8E) was distinct from that of the corresponding fluorescent LCFA (BODIPY-C16) and SYTO59 (Figure 8C). While BODIPY-C16 colocalized with SYTO59 primarily near the nuclear envelope (Figure 8C), very little BODIPY-C16-S-S-CoA colocalized with SYTO59 near the nuclear envelope (Figure 8E). Instead, BODIPY-C16-S-S-CoA colocalized with SYTO59 as both diffusely distributed pixels throughout the nucleoplasm and as bright-punctuate structures within the nucleoplasm (Figure 8E). Finally, in L-FABP-expressing cells the distribution of BODIPY-C16-S-S-CoA colocalized with SYTO59 was brighter, but with similar diffusely and bright-punctuate distributed throughout the nucleoplasm (Figure 8F). The colocalization coefficiencies were red, 0.12 ± 0.01 (mean ± SE, $n = 14$), and green, 0.26 ± 0.02 (mean ± SE, $n = 14$), which indicated that, in the medial cross-sectional plane of L-FABP-expressing L-cells, 26% of the BODIPY-C16-S-S-CoA was colocalized with SYTO59 in nuclei, severalfold higher than in control cells.

In summary, although both fluorescent LCFAs (BODIPY-C12, BODIPY-C16) and fluorescent LCFA-CoA (BODIPY-C16-S-S-CoA) were taken up into nuclei of control L-cells, the pattern of distribution within the nuclei differed markedly. Qualitative analysis suggested that L-FABP expression enhanced the uptake of both fluorescent LCFAs (BODIPY-C12, BODIPY-C16) and fluorescent LCFA-CoA (BODIPY-C16-S-S-CoA) into nuclei to dramatically alter the pattern of fluorescent LCFA (BODIPY-C12, BODIPY-C16) but not fluorescent LCFA-CoA (BODIPY-C16-S-S-CoA) distribution within the nuclei.

Quantitative Analysis of the Time Course of Fluorescent Fatty Acid (BODIPY-C12, BODIPY-C16) and Fluorescent Fatty Acyl CoA (BODIPY-C16-S-S-CoA) Uptake and Distribution into the Nucleoplasm, Nuclear Membrane, and Cytoplasm: Effect of L-FABP Expression. The LSCM images of BODIPY-C12 in control vs L-FABP-expressing cells clearly demonstrate the problem of trying to obtain quantitative information regarding how much BODIPY-C12 was present in the nucleus, much less the nucleoplasm vs nuclear envelope. However, the development of SYTO59 as a DNA binding probe clearly delineated the nuclear DNA, separate from the cytoplasm. Therefore, these characteristics were used to more quantitatively distinguish the distributions of fluorescent LCFA (BODIPY-C12, BODIPY-C16) and fluorescent LCFA-CoA (BODIPY-C16-S-S-CoA) within the nucleoplasm, nuclear envelope membranes, and cytoplasm outside the nucleus (i.e., cytoplasm plus plasma membrane). In control L-cells, these fluorescent molecules were taken up nearly linearly over the 30 min incubation time, and intensities were distributed in the approximate order: cytoplasm $\gg$ nuclear membrane $>$ nucleoplasm (Figure 9).

With increasing incubation time, L-FABP expression dramatically increased the uptake of fluorescent fatty acids (BODIPY-C12, BODIPY-C16) into the nucleoplasm and nuclear membrane. L-FABP enhanced the distribution of the medium-chain BODIPY-C12 into the nucleoplasm and nuclear membranes, but less so into cytoplasm (Figure 9, panels A−C). By 30 min incubation, L-FABP expression increased the BODIPY-C12 uptake by 3.1-, 1.8-, and 1.2-fold into the nucleoplasm, nuclear membrane, and cytoplasm, respectively (Figure 9, panels A−C, and Table 1). Kinetic analysis showed that L-FABP expression increased the initial rate of BODIPY-C12 into whole cells 1.8-fold (Table 1). However, the fold increase was not the same throughout the whole cell. The fold increase was highest for the nucleoplasm (4.8-fold), followed by the nuclear membrane (2.5-fold), and the lowest was the cytoplasm (only 1.4-fold) (Table 1). By 30 min incubation, L-FABP expression increased the BODIPY-C16 uptake by 7.4-, 1.7-, and 2.4-fold in the nucleoplasm, nuclear membrane, and cytoplasm, respectively (Figure 9, panels D−F, and Table 1). Comparisons of the initial rates of uptake demonstrated that L-FABP expression increased the initial rate of BODIPY-C16 uptake into whole cells 2.4-fold (Table 1). Again, the fold increase was not the same throughout the whole cell. The fold increase was highest for the nucleoplasm (7.3-fold), followed by the cytoplasm (2.3-fold), and the lowest was the nuclear membrane (1.6-fold).

L-FABP expression also increased the uptake of fluorescent LCFA-CoA (BODIPY-C16-S-S-CoA) into nuclei. After incubation with BODIPY-C16-S-S-CoA, fluorescence increases of L-FABP-expressing cells were more rapid and reached higher maximum values than in control cells, especially in the nucleoplasm and nuclear membrane. By 30 min incubation, L-FABP expression increased the BODIPY-C16-S-S-CoA uptake by 2.7-, 1.9-, and 1.3-fold in the nucleoplasm, nuclear membrane, and cytoplasm, respectively (Figure 9, panels G−I, and Table 1). Comparison of the 30 min incubation data for BODIPY-C16 and BODIPY-C16-S-S-CoA uptake revealed that, while L-FABP similarly enhanced their uptake into the nuclear membrane, L-FABP targeted the BODIPY-C16 nearly 3- and 2-fold more into the nucleoplasm and cytoplasm, respectively, than BODIPY-C16-S-S-CoA. Comparisons of the initial rates of uptake demonstrated that L-FABP expression increased the rate of BODIPY-C16-S-S-CoA uptake into whole cells 1.5-fold, less than either BODIPY-16 or BODIPY-C12 (Table 1). However, the fold increase was not the same throughout the whole cell. The fold increase in the rate of BODIPY-C16-S-S-CoA was highest for the nucleoplasm (2.5-fold), followed by the

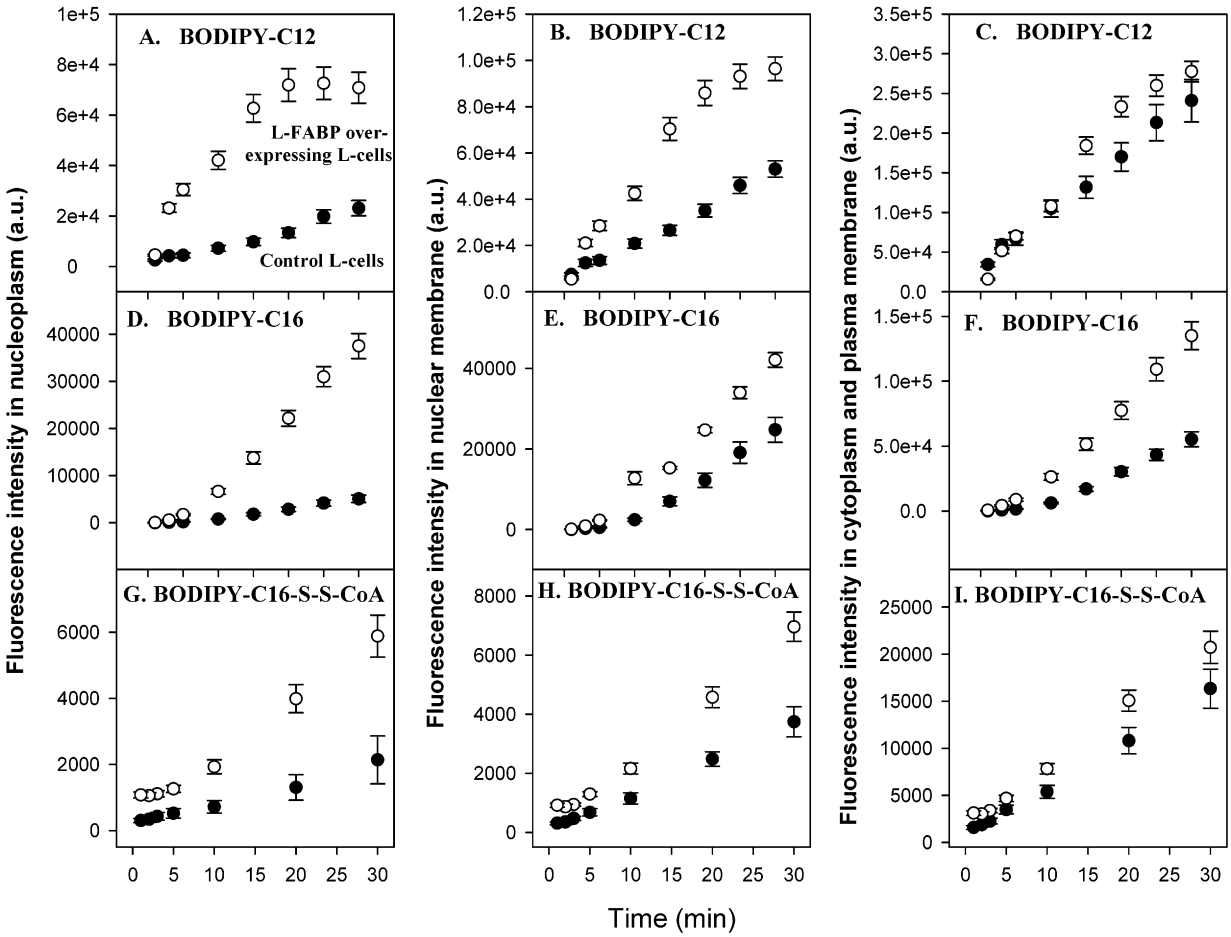

FIGURE 9: Effect of L-FABP expression on fluorescent fatty acid [BODIPY-C12 (panels A−C) and BODIPY-C16 (panels D−F)] and nonhydrolyzable fatty acyl CoA [BODIPY-C16-S-S-CoA (panels G−I)] uptake and distribution: L-FABP-expressing (open circles) and control L-cells (filled circles). Data presented are fluorescence intensity (au) (mean ± SE, $n = 7-22$) in the nucleoplasm (panels A, D, and G), nuclear membrane (panels B, E, and H), and cytoplasm plus plasma membrane (panels C, F, and I).

Table 1: Effect of L-FABP Expression on Intracellular Distribution of Fluorescent LCFA-CoA and LCFA[a]

	initial rate of uptake (fluorescence intensity units/min, mean ± SE)			fold increase in total uptake at 30 min time point
	control L-cell	L-FABP-overexpressing L-cell	fold increase	
BODIPY-C12				
nucleoplasm	700 ± 94 ($n = 12$)	3380 ± 312*** ($n = 19$)	4.8	3.1
nuclear membrane	1540 ± 116 ($n = 12$)	3906 ± 286*** ($n = 19$)	2.5	1.8
cytoplasm	7020 ± 839 ($n = 12$)	10148 ± 556** ($n = 19$)	1.4	1.2
whole cell	9254 ± 921 ($n = 12$)	16867 ± 869*** ($n = 19$)	1.8	
BODIPY-C16				
nucleoplasm	204 ± 33 ($n = 9$)	1488 ± 99*** ($n = 7$)	7.3	7.4
nuclear membrane	1008 ± 129 ($n = 9$)	1643 ± 78** ($n = 7$)	1.6	1.7
cytoplasm	2250 ± 233 ($n = 9$)	5182 ± 407*** ($n = 7$)	2.3	2.4
whole cell	3463 ± 289 ($n = 9$)	8312 ± 425*** ($n = 7$)	2.4	
BODIPY-C16-S-S-CoA				
nucleoplasm	70 ± 20 ($n = 8$)	174 ± 20** ($n = 22$)	2.5	2.7
nuclear membrane	118 ± 13 ($n = 8$)	217 ± 17** ($n = 22$)	1.8	1.9
cytoplasm	510 ± 67 ($n = 8$)	636 ± 54 ($n = 22$)	1.2	1.3
whole cell	690 ± 84 ($n = 8$)	1022 ± 70* ($n = 22$)	1.5	

[a] Values are in arbitrary intensity units and represent the mean ± SE. The number of cells (n) is given in parentheses. These values are significantly different from control L-cells: *, $p < 0.05$; **, $p < 0.01$; ***, $p < 0.001$.

nuclear membrane (1.8-fold), and there was no significant difference for the cytoplasm.

To confirm the suggestion, made by these data, that L-FABP preferentially enhanced the distribution of the LCFAs and LCFA-CoA (BODIPY-C16-S-S-CoA) into the nucleoplasm and nuclear membranes, the results in Figure 9 were presented as percent distribution (Figure 10). For BODIPY-C12, during the entire 30 min incubation time period, the percent distribution in the nucleoplasm and nuclear membrane was always higher in L-FABP-expressing cells, at the expense of the percent distributed in the cytoplasm (Figure 10A−C). For the experiment with BODIPY-C16, during the entire 30 min, compared with the control cells, the percent distributions in L-FABP-expressing

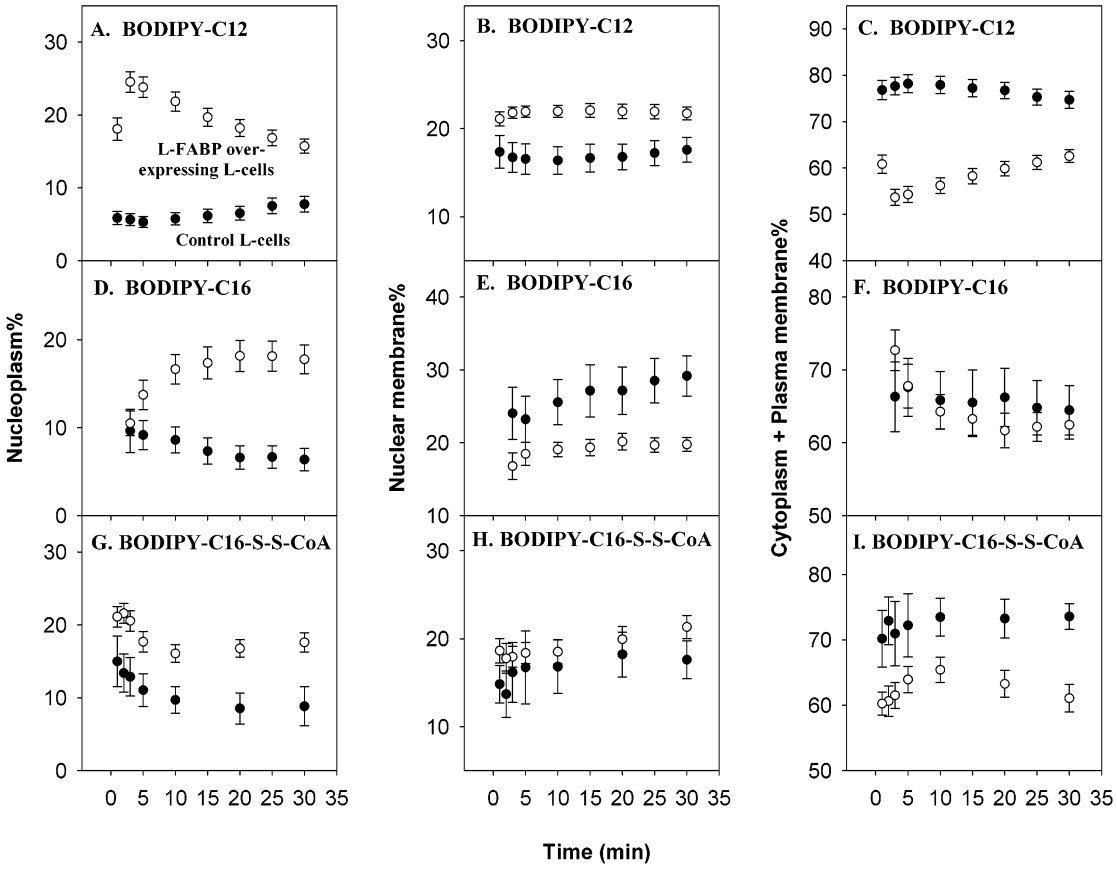

FIGURE 10: Effect of L-FABP expression on percent distribution of fluorescent fatty acids [BODIPY-C12 (panels A−C) and BODIPY-C16 (panels D−F)] and nonhydrolyzable fatty acyl CoA [BODIPY-C16-S-S-CoA (panels G−I)] into L-cell subcellular compartments: L-FABP-expressing (open circles) and control L-cells (filled circles). Data presented are percent fluorescence intensity (mean ± SE, n = 7−22) in the nucleoplasm (panels A, D, and G), nuclear membrane (panels B, E, and H), and cytoplasm plus plasma membrane (panels C, F, and I).

cells were higher in the nucleoplasm, at the expense of lower levels in the nuclear envelope membranes and similar levels in the cytoplasm (Figure 10, panels D−F). For the experiment with BODIPY-C16-S-S-CoA, comparison with the control cells showed that the percent distribution in L-FABP-expressing cells was higher in the nucleoplasm, about the same in the nuclear membrane, and at the expense of the cytoplasm (Figure 10G−I).

In summary, while L-FABP clearly enhanced the uptake of all three probes into the nucleoplasm, nuclear membrane, and cytoplasm, in terms of preference L-FABP was particularly selective with regard to increasing the percent distribution of LCFAs (BODIPY-C12, BODIPY-C16) and LCFA-CoA (BODIPY-C16-S-S-CoA) into the nucleoplasm and, in the case of the medium-chain-length LCFA (BODIPY-C12), also into the nuclear membrane.

Effect of L-FABP Expression on Endogenous LCFA-CoA Pool Size and Endogenous LCFA-CoA Acyl Chain Composition. To resolve whether L-FABP expression increases the LCFA-CoA pool size in L-cell fibroblasts, cells were cultured for 2 days in Higuchi medium with three different supplements: (i) BSA plus no LCFA; (ii) BSA plus linoleic acid; (iii) 10% fetal bovine serum. Fetal bovine serum contains not only small amounts of unesterified LCFA bound to albumin but also large quantities esterified to phospholipids (280 nmol/mg of protein), cholesteryl ester (136 nmol/mg of protein), and triacylglyceride (13 nmol/mg of protein) (Table 2). The medium-chain-length fatty acids (i.e., 14−16 carbons long) represented about 20% of the total while the long-chain fatty acids comprised the remainder. The most common medium- and long-chain fatty acids were 16 and 18 carbons long. At least half of the total esterified LCFAs in the major serum lipid (i.e., phospholipids) were saturated fatty acids, while the cholesteryl esters and triacylglycerides were more enriched in unsaturated LCFAs (Table 2).

In the absence of LCFA in the cell culture medium, L-FABP expression significantly increased the total endogenous LCFA-CoA pool mass (pmol/mg of protein) by 21% ($p < 0.05$) (Figure 11A, total). Furthermore, when individual LCFA-CoAs were resolved by HPLC, L-FABP expression selectively increased the mass of several LCFA-CoAs: C16:1-, C18:0-, C18:1-, and C18:3-CoA (Figure 10A).

As compared to cells grown without LCFA in the medium, when cells were cultured in medium supplemented with linoleic acid (C18:2), the total LCFA-CoA mass was increased by 2.4-fold from 19 to 45 pmol/mg of protein (Figure 11B vs Figure 11A, total open bars). Furthermore, the culture with C18:2 selectively enriched the LCFA-CoA pool mass by 30% for C18:2-CoA and by 2.5-fold for C18:0-CoA plus C18:1-CoA plus C18:2-CoA plus C18:3-CoA (Figure 11B vs Figure 11A). L-FABP overexpression did not further increase the total LCFA-CoA pool mass in cells cultured with medium supplemented with linoleic acid (Figure 11B). However, HPLC analysis of individual LCFA-CoAs revealed that L-FABP expression elicited significant changes in the types of acyl groups within the LCFA-CoA

Table 2: Fetal Bovine Serum Phospholipid, Cholesteryl Ester, and Triacylglyceride Fatty Acid Mass and Composition and Fatty Acid Ratios[a]

	mass (nmol/mg of protein)		
fatty acid	phospholipid	cholesteryl ester	triacyl-glyceride
14:0	ND	1.59 ± 0.18	ND
14:1 n-5	ND	1.15 ± 0.08	ND
16:0	52.76 ± 3.93	17.52 ± 1.33	1.57 ± 0.26
16:1 n-7	1.19 ± 0.19	8.22 ± 0.85	ND
18:0	74.35 ± 3.92	4.46 ± 0.52	0.98 ± 0.01
18:1 n-9	52.23 ± 3.37	40.08 ± 3.85	2.49 ± 0.39
18:1 n-6	24.75 ± 1.37	18.66 ± 1.75	1.46 ± 0.25
18:2 n-6	5.76 ± 0.57	17.13 ± 1.71	1.19 ± 0.15
18:3 n-6	ND	0.31 ± 0.05	ND
20:0	0.73 ± 0.06	0.71 ± 0.09	ND
20:1	3.39 ± 0.24	ND	ND
20:1 n-7	2.04 ± 0.11	0.55 ± 0.04	ND
20:2 n-6	3.73 ± 0.25	1.31 ± 0.13	1.25 ± 0.07
20:3 n-6	9.72 ± 0.49	1.38 ± 0.21	ND
20:4 n-6	ND	18.32 ± 2.10	2.5 ± 0.3
22:0	19.31 ± 1.12	ND	ND
22:1 n-7	0.28 ± 0.05	0.27 ± 0.03	ND
24:0	0.49 ± 0.04	1.13 ± 0.16	0.33 ± 0.06
22:4 n-6	4.44 ± 0.32	0.53 ± 0.02	0.66 ± 0.05
24:1 n-9	13.36 ± 0.66	0.78 ± 0.08	ND
22:6 n-3	11.09 ± 0.66	1.95 ± 0.29	0.47 ± 0.05
saturated/protein	147.63 ± 5.66	25.40 ± 1.45	2.88 ± 0.29
unsaturated/protein	134.59 ± 3.87	110.63 ± 5.11	10.02 ± 0.58
MUFA/protein	98.48 ± 3.71	69.70 ± 4.32	3.95 ± 0.46
PUFA/protein	36.11 ± 1.09	40.93 ± 2.74	6.07 ± 0.35
ratios (nmol/nmol)			
unsaturated/ saturated	0.91 ± 0.04	4.36 ± 0.32	3.48 ± 0.40
PUFA/MUFA	0.37 ± 0.02	0.59 ± 0.05	1.54 ± 0.2

[a] Values represent the means ± standard error, $n = 3-6$.

pool: decreased mass (Figure 11B) of C16:0-CoA and C20:0-CoA.

Finally, when cells were cultured in medium supplemented with 10% fetal bovine serum and analyzed by HPLC, the total LCFA-CoA mass was increased 1.2-fold from 19 to 23 pmol/mg of protein (Figure 11C vs Figure 11A, total open bars). L-FABP expression did not significantly increase the total LCFA-CoA pool mass (Figure 11C). However, HPLC analysis of individual LCFA-CoAs revealed that L-FABP expression significantly increased the mass (Figure 11C) of C18:0-CoA.

In summary, L-FABP expression increased the total LCFA-CoA pool mass only when the cells were cultured in the absence of LCFA in the medium. However, under all conditions examined, L-FABP expression exerted subtle but significant effects on the acyl chain distribution within the LCFA-CoA pool.

Estimated Concentrations of Fluorescent Long-Chain Fatty Acids and Fatty Acyl CoAs in Nuclei of Living Cells. L-FABP-expressing and control L-cells were incubated with BODIPY-C12, BODIPY-C16, or BODIPY-C16-S-S-CoA (final concentration 0.1 μM) for 30 min. The concentration of these fluorescent molecules (Table 3) in control and L-FABP-expressing L-cells was calculated as described in Experimental Procedures. The concentrations of BODIPY-C12 in the nucleoplasm and the whole nucleus of L-FABP-expressing L-cells were significantly higher than in control L-cells ($p < 0.01$, Student's *t*-test). The calculated concentrations of BODIPY-C16 in the nucleoplasm, whole nucleus, and cytoplasm plus plasma membrane were all higher than BODIPY-C12 due to higher uptake. Furthermore, L-FABP expression increased the calculated concentrations of BODIPY-C16 in the nucleoplasm, whole nucleus, and cytoplasm plus plasma membrane as compared to control L-cells. Finally, the concentrations of BODIPY-C16-S-S-CoA in the different subcellular compartments were all much lower (i.e., in the nanomolar range) than those of the respective BODIPY-C16 or BODIPY-C12 (Table 3). L-FABP overexpression significantly increased BODIPY-C16-S-S-CoA concentrations in the nucleoplasm and whole nucleus by 2.7- and 2.2-fold, respectively, while levels in cytoplasm plus plasma membrane were not significantly altered (Table 3).

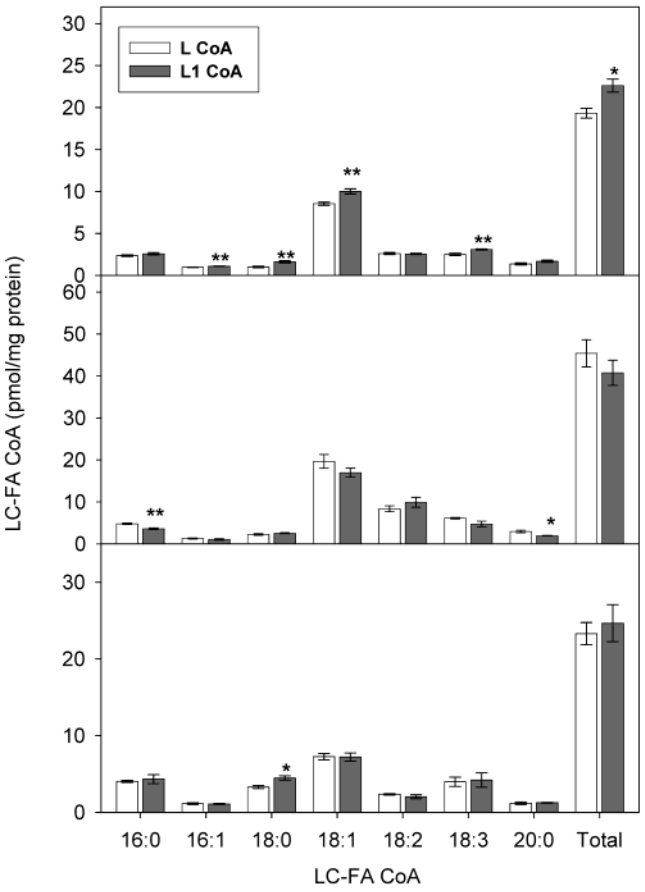

FIGURE 11: Effect of L-FABP expression on LCFA-CoA pool size in L-cells cultured in the absence of fatty acid (panel A), in L-cells cultured in the presence of linoleic acid (C18:2) (panel B), and in L-cells cultured in the presence of 10% fetal bovine serum (panel C). The cell culture media were changed to the corresponding media 1 day before the data collection. The LCFA-CoAs were extracted from the cells (with added internal standard) by solid-phase extraction, converted to fluorescent analogue etheno CoAs, and quantitated by HPLC as described in Experimental Procedures. Key: L-FABP-expressing (filled columns) and control L-cells (open columns). Data presented are the mean ± SE, $n = 5$. The asterisks indicate a significant difference from control L-cells by Student's *t*-test (*, $p < 0.05$; **, $p < 0.01$).

DISCUSSION

A broad range of studies performed in vitro, in transfected cells, and in animals indicate that fatty acids (LCFAs) and their acyl CoA derivatives (LCFA-CoAs) may be important physiological regulators of nuclear receptors, especially PPARα (reviewed in refs *2* and *37*−*41*) and HNF4α (reviewed in refs *5* and *12*). PPARα regulates the transcrip-

Table 3: Effect of L-FABP Expression on Cellular Concentration of Fluorescent LCFA-CoAs and LCFAs[a]

	concentration (μM)					
	control L-cells			L-FABP-expressing L-cells		
	nucleoplasm	whole nucleus	cytoplasm + plasma membrane	nucleoplasm	whole nucleus	cytoplasm + plasma membrane
BODIPY-C12	0.039 ± 0.005 ($n = 12$)	0.319 ± 0.044 ($n = 12$)	0.542 ± 0.075 ($n = 12$)	0.121 ± 0.016** ($n = 19$)	0.702 ± 0.097** ($n = 19$)	0.650 ± 0.090 ($n = 19$)
BODIPY-C16	0.068 ± 0.010 ($n = 9$)	1.46 ± 0.21 ($n = 9$)	0.98 ± 0.14 ($n = 9$)	0.50 ± 0.07** ($n = 7$)	3.94 ± 0.57** ($n = 7$)	2.35 ± 0.34 ** ($n = 7$)
BODIPY-C16-S-S-CoA	$(3.26 \pm 0.39) \times 10^{-3}$ ($n = 8$)	0.0229 ± 0.0027 ($n = 8$)	0.0373 ± 0.0045 ($n = 8$)	$(8.8 \pm 1.1) \times 10^{-3}$** ($n = 22$)	0.0504 ± 0.0059* ($n = 22$)	0.0485 ± 0.0059 ($n = 22$)

[a] Concentrations were calculated as described in Experimental Procedures. The data represent means ± SE (n). **: significantly different from the control L-cells, $p < 0.01$, Student's t-test.

tion of multiple genes involved in fatty acid uptake (*42*), fatty acid oxidation (*43*), and signaling (*44*) and may play a role in obesity and lipid disorders (*39*, *45*, *46*). PPARα gene ablation results in abnormal LCFA oxidation, altered serum lipoprotein patterns, obesity, and steatosis (*47*−*51*). With regard to HNF4α, a cDNA microarray (*52*) and other analyses (reviewed in ref *11*) have shown that nearly half of the classified genes upregulated by HNF4α are involved in LCFA, bile acid, and glucose metabolism (*53*−*56*). Conditional HNF4α gene ablation in liver decreases expression of genes involved in VLDL secretion (apoCIII, apoCII, apoB, microsomal triglyceride transfer protein), lowers serum VLDL level, decreases serum triglyceride and cholesterol, and induces lipid accumulation in liver (*3*). In humans, mutations in HNF4α cause maturity-onset diabetes of the young (MODY-1), characterized by impaired triacylglycerol metabolism and insulin secretion and significantly reduced serum levels of apoCIII, apoAII, lp(a), and triacylglycerol (*57*−*59*). Nevertheless, despite the importance of LCFAs and LCFA-CoAs in regulating the transcriptional activity of PPARα and HNF4α mediating these physiological effects, almost nothing is known regarding the presence of these ligands in the nucleus, the distribution of these ligands within the nucleus (nucleoplasm versus nuclear envelope), and factors regulating the distribution of these ligands to these nuclear compartments. The work presented herein makes several important contributions that begin to address these questions.

First, immunofluorescence imaging demonstrated that in L-FABP-expressing cells the L-FABP was present in nuclei. Intense staining of L-FABP was best obtained in the nucleoplasm when cells were labeled with a single antibody, i.e., anti-L-FABP (Figure 2A). Nuclear staining with anti-L-FABP appeared less intense in dual immunolabeled cells, i.e., anti-L-FABP and anti-PPARα (Figure 3C), because L-FABP-expressing cells contained much less PPARα than L-FABP, thereby requiring adjustment in the relative proportions of anti-L-FABP antibody used. The detection of L-FABP within nuclei was consistent with earlier reports demonstrating the presence of L-FABP in isolated nuclei purified by cellular subfractionation (*32*), in immunogold-labeled liver hepatocytes (*32*), and in immunofluorescence-labeled transfected embryonic stem cells expressing L-FABP (*33*). On the basis of total intensities of L-FABP-expressing cells immunostained only with anti-L-FABP antibody, on the middle cross section, the nucleus contained about 25% of total L-FABP, qualitatively consistent with earlier reports (*32*, *33*). When these intensities, along with estimated volumes of the respective compartments, were used to calculate the molar concentration of L-FABP as described in Experimental Procedures, the level of L-FABP in the nucleus (43.2 ± 2.2 μM) was only slightly lower than in the cytoplasm (51.4 ± 1.5 μM). In tissues active in LCFA metabolism (i.e., liver, heart, adipose) FABPs represent 2−5% of the cytosolic protein (0.2−1.0 mM), such that L-FABP concentrations in liver cells, for example, are 200−400 μM (*15*, *60*). Since L-FABP accounts for 0.4% of the soluble protein in L-FABP-expressing L-cells, the cytoplasmic concentration of L-FABP near 51 μM was in the expected range. These data presented herein for the first time provide direct evidence that L-FABP is present in nuclei at concentrations similar to those in the cytoplasm. However, the distributions of L-FABP in these compartments differed markedly, diffuse in cytoplasm vs intensely staining structures within the nucleoplasm and less at the nuclear envelope.

Second, it was shown that in L-FABP-expressing cells a small portion of L-FABP was colocalized with PPARα. PPARα, and less so L-FABP, was most highly distributed in the nucleus near the nuclear envelope and also in bright areas possibly reflecting nucleoli. In the middle cross-sectional plane of L-FABP-expressing L-cells, approximately 30% of PPARα and 23% of the L-FABP were colocalized, primarily in nuclei. Thus, although L-cells are a transformed cell line (*61*−*63*), L-FABP and PPARα distributed in transfected L-cells in patterns similar to those observed in normal cells and tissues. Consistent with the possibility that L-FABP binds to PPARα in the nucleus, both pull-down assay and immunocoprecipitation demonstrate that L-FABP interacts directly with PPARα (*18*). In addition, a mammalian two-hybrid system confirmed that L-FABP interacted with PPARα (and PPARγ but not with PPARβ) by protein−protein contacts (*18*). The data presented herein for the first time provide direct evidence that L-FABP and PPARα colocalize in the nucleus, both near the nuclear envelope and in punctate areas resembling nucleoli, in L-FABP-expressing L-cells.

Third, the use of the DNA binding dye SYTO59 for the first time allowed clear demonstration that LCFAs are present in the nucleoplasm as compared to the nuclear envelope membrane region of living cells. Studies with nuclei isolated by subcellular fractionation do not distinguish this possibility and, furthermore, are potentially complicated by LCFA redistribution or lipolytic release during subcellular fractionation (*60*, *64*−*66*). Likewise, while an earlier LSCM report from this laboratory showed that LCFAs appeared in nuclei, the lack of a nuclear DNA marker precluded accurate

discrimination of LCFAs present in the nuclear envelope versus those localized in the nucleoplasm (*19*). The work presented herein addressed the issue through use of nonhydrolyzable or poorly metabolizable fluorescent LCFAs (BODIPY-C12 and BODIPY-C16) (*19*) and SYTO59, a DNA binding probe that clearly demarcated the nucleoplasm in LSCM images of living L-cells. In nuclei from control cells, both LCFAs distributed primarily to nuclear envelope membranes (18−30% of total LCFA taken up), 3−4-fold more than to the nucleoplasm (5−9% of total taken up). The L-cell fibroblasts contain no detectable L-FABP and very little other cytosolic proteins capable of binding LCFAs (reviewed in refs *15* and *67*). Thus, these data show that although exogenous LCFAs are taken up into the nuclear envelope region, they are weakly internalized into the nucleoplasm. Nucleoplasmic concentrations of BODIPY-C12, BODIPY-C16, and endogenous LCFA (assuming the endogenous LCFA has the same distribution as the fluorescent analogues) were estimated at 0.04, 0.07, and 0.72 μM. These concentrations are well within the range of affinities of PPARα for LCFAs (*6*) but not of HNF4α, which has weak affinity for LCFAs (*11*, *12*).

Fourth, for the first time LCFA-CoA was directly visualized in nuclei of living cells. After 30 min uptake, on the middle cross-sectional plane, about 8% and 16% of BODIPY-C16-S-S-CoA was distributed to the nucleoplasm and nuclear membrane, respectively. The use of the DNA binding dye SYTO59 and real-time LSCM imaging demonstrated for the first time that LCFA-CoA in nuclei is nearly evenly distributed to the nucleoplasm (10−15% of total LCFA-CoA taken up) as compared to the nuclear envelope membrane region (10−15% of total taken up) in control L-cells. Studies with nuclei isolated by subcellular fractionation do not distinguish this possibility. Thus, the distribution of LCFA-CoA within the nuclei differed markedly from that of LCFA. While LCFA-CoA was primarily punctate in the nucleoplasm, LCFA was diffusely distributed through the nucleoplasm. These data suggest that the nucleoplasm contains more LCFA-CoA than LCFA binding sites, possibly reflecting the specificity of nuclear binding proteins. Nucleoplasmic concentrations of BODIPY-C16-S-S-CoA and endogenous LCFA-CoA (assuming the endogenous LCFA-CoA has the same distribution as the fluorescent analogues) were estimated at 3.3 and 3.1 nM. These concentrations are well within the range of affinities of HNF4α (*11*, *12*) and PPARα (*8*, *9*) for LCFA-CoAs.

It is important to consider whether the distribution of the BODIPY-S-S-CoA to nuclei reflects that of naturally occurring LCFA-CoA. The hydrolyzable, naturally occurring LCFA-CoAs all are very rapidly metabolized, are subject to the action of hydrolases, redistribute among different organelles during subcellular fractionation, and preclude discrimination of LCFA-CoAs localized to the nuclear membranes vs nucleoplasm. Since naturally occurring, metabolizable LCFA-CoAs are not fluorescent, it is not possible to image their distribution in nuclei in real time in living cells. In contrast, incubation of the nonhydrolyzable BODIPY-C16-S-S-CoA with L-cells for 30 min resulted in 2.1% of the BODIPY-C16-S-S-CoA fluorescence distributed to nucleoplasm and 17.4% in the nuclear membrane (total of 20% in the whole nucleus) in real time in living cells. A priori, it is not possible to directly compare the distribution of BODIPY-C16-S-S-CoA with that of naturally occurring metabolizable LCFA-CoAs in living cells. To date, the only comparisons that can be made are with purified rat liver nuclei, whose LCFA-CoA content was 0.32 nmol/g wet weight (*68*). It was reported that the total LCFA-CoA concentration of rat liver cells ranges from 15 to 83 nmol/g wet weight (reviewed in refs *67* and *69*). Therefore, the purified rat liver nuclei contain only 0.39−2% of total metabolizable LCFA-CoA. The purified nuclei data would suggest that either (i) BODIPY-C16-S-S-CoA poorly reflects the distribution of LCFA-CoA in the nucleus or (ii) LCFA-CoA is significantly degraded (hydrolyzed, transesterified) or lost (e.g., by redistribution to other organelles) during isolation of nuclei from rat liver. Consistent with the latter possibility, about 5% of the radiolabeled poorly metabolizable LCFA-CoA ([1-^{14}C]tetradecylthioacetyl-CoA) was retained in purified rat liver nuclei as compared to whole liver. Although these represent only limited comparisons, the data suggest that BODIPY-C16-S-S-CoA distribution to nuclei has relevance to that of naturally occurring LCFA-CoAs, representing an equilibrium or maximal distribution in the absence of competition from degradation by hydrolysis and transesterification to other lipids.

Fifth, L-FABP enhanced the uptake and selective distribution of fluorescent LCFA into nucleoplasm and nuclear envelope membranes of L-FABP-expressing L-cells. L-FABP had high affinity for BODIPY-C12 ($K_i = 10.1 \pm 2.5$ nM) and BODIPY-C16 ($K_i = 20.7 \pm 1.5$ nM) in the same range as that for other LCFAs (reviewed in ref *15*). L-FABP expression (0.4% of cytosolic protein) increases the total LCFA binding capacity of L-cell cytoplasm by nearly 4-fold (*22*). Although L-cells contain low levels of endogenous FABP (0.12% of cytosolic protein) that does not cross-react with antisera to L-FABP, L-FABP expression does not alter endogenous FABP expression in the transfected cells (*22*). SYTO59, a fluorescent DNA stain, was used to show that L-FABP expression quantitatively and selectively severalfold enhanced the uptake of fluorescent LCFAs (BODIPY-C12, BODIPY-C16) into nucleoplasm, in the case of BODIPY-C16 by nearly an order of magnitude. Several lines of evidence support the possibility that L-FABP enhances transport of LCFA to the nucleus and into the nucleoplasm: (i) L-FABP is sufficiently small (14 kDa) to pass through nuclear pores and was detected in nucleoplasm of L-FABP-expressing cells (see above and ref *33*) (*32*). (ii) L-FABP has two LCFA binding sites, with the high-affinity binding site exhibiting K_ds as low as 8−18 nM for LCFAs (*16*). These affinities are well within the range of the affinities reported for PPARα binding LCFAs (*6*) and nuclear LCFA concentrations (*19*). (iii) L-FABP increases the diffusion of naturally occurring and synthetic fluorescent LCFAs in the cytoplasm (*15*, *70*, *71*). (iv) In vitro studies show that L-FABP containing bound LCFA, but not unliganded L-FABP, cotransports LCFA to isolated nuclei (*60*). These data suggest that L-FABP/LCFA complexes, but not free LCFAs, cotransport bound LCFA to highly purified nuclei isolated by subcellular fractionation (*60*).

Sixth, L-FABP expression also severalfold enhanced the uptake and selective distribution of BODIPY-C16-S-S-CoA into the nucleoplasm. L-FABP is known to bind two LCFA-CoAs (at the same sites as LCFAs) (*16*). Although early LCFA-CoA radioligand binding studies suggested that L-

FABP has only weak affinity (micromolar K_ds) (reviewed in ref *15*), subsequent fluorescence binding assays demonstrated that the L-FABP high-affinity binding site exhibits K_ds as low as 8−10 nM for LCFA-CoAs (*16*), well within the range of nuclear LCFA-CoA levels (Table 3 and ref *72*) (*73*) and affinities reported for PPARα binding LCFA-CoAs (*8*, *9*) or HNF4α (*11*) binding LCFA-CoAs (*12*). Although it is not known whether L-FABP enhances intracellular transport/diffusion of LCFA-CoAs, the present data demonstrate that L-FABP enhances targeting of LCFA-CoA to the nucleus, specifically into the nucleoplasm therein.

Seventh, L-FABP expression increased the size of the endogenous LCFA-CoA pool as well as the acyl chain length distribution of the LCFA-CoAs. The L-FABP high-affinity binding site exhibits K_ds as low as 8−10 nM for LCFA-CoAs (*16*), and L-FABP overexpression increased the LCFA-CoA pool size by nearly 20%. Similarly, acyl CoA binding protein (ACBP) binds LCFA-CoA with even higher affinity (0.6−4 nM K_ds) (*72*, *74*, *75*) and, when overexpressed in yeast, increased by nearly 2-fold the LCFA-CoA pool size as well as altered the LCFA-CoA acyl chain distribution (*76*). While it is not known whether ACBP expression enhances LCFA-CoA targeting to nuclei, the data presented herein clearly showed that L-FABP enhanced LCFA-CoA distribution to the nucleus, especially nucleoplasm.

Although the total lengths of the BODIPY-C12 and BODIPY-C16 fatty acid probe molecules (Figure 1) were well within those of the naturally occurring LCFAs occurring in serum (Table 2), extraction and HPLC analysis showed that L-FABP expression affected endogenous total LCFA-CoA levels (Figure 11) less than that obtained by measuring the distribution of BODIPY-C16-S-S-CoA determined by confocal imaging (Figure 9). These differences may be explained on the basis of two effects: (i) The extraction and HPLC analysis were performed on whole cells. In contrast, the confocal imaging of BODIPY-C16-S-S-CoA was performed on subcellular compartments to show that L-FABP expression had a large effect on BODIPY-C16-S-S-CoA accumulation in the nucleoplasm and nuclear membranes (Figure 9G,H). The effect of L-FABP expression on BODIPY-C16-S-S-CoA distribution to cytoplasm plus plasma membrane was much smaller (Figure 9I). When taken together for the whole cell image, this suggested that L-FABP had a greater effect on redistribution of BODIPY-C16-S-S-CoA within cells (Figure 9, Table 1) than on determining the absolute LCFA-CoA level in the cell (Figure 11). (ii) L-FABP enhances the utilization of naturally occurring LCFA-CoA by fatty acyl CoA acyltransferases (*15*, *77*). Since BODIPY-C16-S-S-CoA is not metabolizable, L-FABP cannot enhance its transacylation. This would suggest that L-FABP increased BODIPY-C16-S-S-CoA uptake and redistribution within the cell independent of factors that would lower LCFA-CoA levels (i.e., BODIPY-C16-S-S-CoA was not metabolized). In contrast, while L-FABP does not enhance LCFA-CoA formation (*78*), it does enhance transacylation of naturally occurring LCFA-CoAs (*15*, *22*, *77*). Therefore, the magnitude of the effect of L-FABP on the cellular total level of a nonmetabolizable LCFA-CoA (e.g., BODIPY-C16-S-S-CoA) was expected to differ from that on metabolizable LCFA-CoAs.

In summary, the results presented herein for the first time demonstrated that LCFA-CoA, as well as LCFA, is localized in the nucleoplasm and nuclear membrane of living cells. Thus, earlier suggestions regarding the presence of LCFA-CoAs (*68*) and unesterified LCFA in nuclei (isolated by subcellular fractionation) were not simply due to artifacts of nuclear isolation or hydrolytic cleavage of esterified lipids to release LCFAs (*64*, *79*, *80*). The 23−30% colocalization of L-FABP and PPARα as well as L-FABP-mediated enhancement of LCFA-CoA as well as LCFA targeting to nuclei, especially nucleoplasm, suggested that L-FABP may serve to shuttle LCFAs and LCFA-CoAs to and/or into the nucleus for donating the ligands to PPARα. The fatty acid shuttling function of L-FABP could be similar to that of CRBP, which shares structural homology with L-FABP, and CTBP (*81*). Since L-FABP expression is regulated by fatty acid-induced PPARα transcriptional activity (*7*), L-FABP may also regulate its own transcription by enhancing LCFA and/or LCFA-CoA targeting to the nucleus. Thus, by altering the distribution of intracellular LCFAs and LCFA-CoAs to the nucleus, L-FABP may therein affect transcription of many genes involved in LCFA metabolism. Furthermore, it is important to note that L-FABP may also provide a specific pool of LCFAs and LCFA-CoAs for nuclear utilization to modify the activity of certain nuclear enzymes, including DNA nucleotidase and DNA-dependent RNA polymerase (*60*) as well as DNA polymerases (*82*) and DNA topoisomerase II (*83*, *84*). Taken together, these data suggest that, by regulating the distribution of fatty acids and acyl CoAs to the nucleus, L-FABP may modulate the activities of LCFA and LCFA-CoA sensitive enzymes and transcription factors therein.

REFERENCES

1. Jump, D. B., Ren, B., Clarke, S. D., and Thelen, A. (1995) Effects of fatty acids on hepatic gene expression, *Prostaglandins, Leukotrienes Essent. Fatty Acids 52*, 107−111.
2. Xu, H. E., Lambert, M. H., Parks, D. J., Blanchard, S. G., Brown, P. J., Sternbach, D. D., Lehmann, J. M., Wisely, G. B., Willson, T. M., Kliewer, S. A., and Milburn, M. V. (1999) Molecular recognition of fatty acids by peroxisome proliferator-activated receptors, *Mol. Cell 3*, 397−403.
3. Hayhurst, G. P., Lee, Y. H., Lambert, G., Ward, J. M., and Gonzalez, F. J. (2001) Hepatocyte nuclear factor 4alpha (nuclear receptor 2A1) is essential for maintenance of hepatic gene expression and lipid homeostasis, *Mol. Cell. Biol. 21*, 1393−1403.
4. Patel, D. D., Knight, B. L., Soutar, A. K., Gibbons, G. F., and Wade, D. P. (2000) The effect of peroxisome proliferator activated receptor alpha on the activity of the cholesterol-7alpha-hydroxylase gene, *Biochem. J. 351*, 747−753.
5. Hertz, R., Magenheim, J., Berman, I., and Bar-Tana, J. (1998) Fatty acyl-CoA thioesters are ligands of hepatic nuclear factor-4α, *Lett. Nat. 392*, 512−516.
6. Lin, Q., Ruuska, S. E., Shaw, N. S., Dong, D., and Noy, N. (1999) Ligand selectivity of the peroxisome proliferator-activated receptor α, *Biochemistry 38*, 185−190.
7. Ellinghaus, P., Wolfrum, C., Assmann, G., Spener, F., and Seedorf, U. (1999) Phytanic acid activates the peroxisome proliferator-activated receptor alpha (PPARalpha) in sterol carrier protein-2-/sterol carrier protein x-deficient mice, *J. Biol. Chem. 274*, 2766−2772.
8. Elholm, M., Dam, I., Jorgenesen, C., Krogsdam, A.-M., Holst, D., Kratchamarova, I., Gottlicher, M., Gustafsson, J. A., Berge, R. K., Flatmark, T., Knudsen, J., Mandrup, S., and Kristiansen, K. (2001) Acyl CoA esters antagonize the effects of ligands on peroxisome proliferator activated receptor a conformation, DNA binding, and interaction with cofactors, *J. Biol. Chem. 276*, 21410−21416.
9. Jorgensen, C., Krogsdam, A.-M., Kratchamarova, I., Willson, T. M., Knudsen, J., Mandrup, S., and Kristiansen, K. (2002)

Opposing effects of fatty acids and acyl-CoA esters on conformation and cofactor recruitment of peroxisome proliferator activated receptors, *Ann. N.Y. Acad. Sci. 967*, 431−439.
10. Bogan, A. A., Dallas-Yang, Q., Ruse, M. D., Maeda, Y., Jiang, G., Nepomuceno, L., Scanlan, T. S., Cohen, F. E., and Sladek, F. M. (2000) Analysis of protein dimerization and ligand binding of orphan receptor HNF4α, *J. Mol. Biol. 302*, 831−851.
11. Petrescu, A. D., Hertz, R., Bar-Tana, J., Schroeder, F., and Kier, A. B. (2002) Ligand specificity and conformational dependence of the hepatic nuclear factor-4alpha (HNF-4α), *J. Biol. Chem. 277*, 23988−23999.
12. Hertz, R., Ben-Naim, M., Petrescu, A., Kalderon, B., Berman, I., Eldad, N., Schroeder, F., and Bar-Tana, J. (2003) Rescue of MODY-1 by agonist ligands of HNF4alpha, *J. Biol. Chem.* (in press).
13. Wisely, G. B., Miller, A. B., Davis, R. G., Thornquest, A. D., Johnson, R., Spitzer, T., Sefler, A., Shearer, B., Moore, J. T., Miller, A. B., Willson, T. M., and Williams, S. P. (2002) Hepatocyte nuclear factor 4 is a transcription factor that constitutively binds fatty acids, *Structure 10*, 1225−1234.
14. Dhe-Paganon, S., Duda, K., Iwamoto, M., Chi, Y.-I., and Shoelson, S. E. (2002) Crystal structure of the HNF4alpha ligand binding domain in complex with endogenous fatty acid ligand, *J. Biol. Chem. 277*, 37973−37976.
15. McArthur, M. J., Atshaves, B. P., Frolov, A., Foxworth, W. D., Kier, A. B., and Schroeder, F. (1999) Cellular uptake and intracellular trafficking of long chain fatty acids, *J. Lipid Res. 40*, 1371−1383.
16. Frolov, A., Cho, T. H., Murphy, E. J., and Schroeder, F. (1997) Isoforms of rat liver fatty acid binding protein differ in structure and affinity for fatty acids and fatty acyl CoAs, *Biochemistry 36*, 6545−6555.
17. Schroeder, F., Jolly, C. A., Cho, T. H., and Frolov, A. A. (1998) Fatty acid binding protein isoforms: structure and function, *Chem. Phys. Lipids 92*, 1−25.
18. Wolfrum, C., Borrmann, C. M., Borchers, T., and Spener, F. (2001) Fatty acids and hypolipidemic drugs regulate PPARalpha and PPARgamma gene expresion via L-FABP: a signaling path to the nucleus, *Proc. Natl. Acad. Sci. U.S.A. 98*, 2323−2328.
19. Huang, H., Starodub, O., McIntosh, A., Kier, A. B., and Schroeder, F. (2002) Liver fatty acid binding protein targets fatty acids to the nucleus: real-time confocal and multiphoton fluorescence imaging in living cells, *J. Biol. Chem. 277*, 29139−29151.
20. Ruoho, A. E., Woldegiorgis, G., Kobayashi, C., and Shrago, E. (1989) Specific labeling of beef heart mitochondrial ADP/ATP carrier with N-(3-iodo-4-azidophenylpropionamido)cysteinyl- 5-(2′-thiopyridyl)cysteine-coenzyme A (ACT-CoA), a newly synthesized 125I-coenzyme A derivative photolabel, *J. Biol. Chem. 264*, 4168−4172.
21. Atshaves, B. P., Storey, S., McIntosh, A. L., Petrescu, A. D., Lyuksyutova, O. I., Greenberg, A. S., and Schroeder, F. (2001) Sterol carrier protein-2 expression modulates protein and lipid composition of lipid droplets, *J. Biol. Chem. 276*, 25324−25335.
22. Jefferson, J. R., Slotte, J. P., Nemecz, G., Pastuszyn, A., Scallen, T. J., and Schroeder, F. (1991) Intracellular sterol distribution in transfected mouse L-cell fibroblasts expressing rat liver fatty acid binding protein, *J. Biol. Chem. 266*, 5486−5496.
23. Higuchi, K. (1970) An improved chemically defined culture medium for strain L mouse cells based on growth responses to graded levels of nutrients including iron and zinc, *J. Cell. Physiol. 75*, 65−72.
24. Voet, D., and Voet, J. G. (1990) in *Biochemistry*, pp 1086−1176, John Wiley & Sons, New York.
25. Martin, G. G., Huang, H., Atshaves, B. P., Binas, B., and Schroeder, F. (2003) Ablation of the liver fatty acid binding protein gene decreases fatty acyl CoA binding capacity and alters fatty acyl CoA pool distribution in mouse liver, *Biochemistry 42*, 11520−11532.
26. Deutsch, J., Grange, E., Rapoport, S. I., and Purdon, A. D. (1994) Isolation and quantitation of long-chain acyl-coenzyme A esters in brain tissue by solid-phase extraction, *Anal. Biochem. 220*, 321−323.
27. Larson, T. R., and Graham, I. A. (2001) A novel technique for the sensitive quantification of fatty acyl CoA esters from plant tissues, *Plant J. 25*, 115−125.
28. Wieland, M., Chehroudi, B., Textor, M., and Brunette, D. M. (2002) Use of Ti-coated replicas to investigate the effects on fibroblast shape of surfaces with varying roughness and constant chemcial composition, *J. Biomed. Mater. Res. 60*, 434−444.
29. Gosslau, A., Dittrich, W., Willig, A., and Jaros, P. P. (2001) Cytological effects of platelet derived growth factor on mitochondrial ultrastructure in fibroblasts, *Comp. Biochem. Physiol., Part A: Mol. Integr. Physiol. 128*, 241−249.
30. Jefferson, J. R., Powell, D. M., Rymaszewski, Z., Kukowska-Latallo, J., and Schroeder, F. (1990) Altered membrane structure in transfected mouse L-Cell fibroblasts expressing rat liver fatty acid-binding protein, *J. Biol. Chem. 265*, 11062−11068.
31. Atshaves, B. P., Storey, S. M., Petrescu, A. D., Greenberg, C. C., Lyuksyutova, O. I., Smith, R., and Schroeder, F. (2002) Expression of fatty acid binding proteins inhibits lipid accumulation and alters toxicity in L-cell fibroblasts, *Am. J. Physiol. 283*, C688−C703.
32. Bordewick, U., Heese, M., Borchers, T., Robenek, H., and Spener, F. (1989) Compartmentation of hepatic fatty-acid-binding protein in liver cells and its effect on microsomal phosphatidic acid biosynthesis, *Biol. Chem. Hoppe-Seyler 370*, 229−238.
33. Schroeder, F., Atshaves, B. P., Starodub, O., Boedeker, A. L., Smith, R., Roths, J. B., Foxworth, W. B., and Kier, A. B. (2001) Expression of liver fatty acid binding protein alters growth and differentiation of embryonic stem cells, *Mol. Cell. Biochem. 219*, 127−138.
34. Zheng, G. Q., Hu, X., Cassady, J. M., Paige, L. A., and Geahlen, R. L. (1994) Synthesis of myristoyl CoA analogues and myristoyl peptides as inhibitors of myristoyl CoA:protein N-myristoyltransferase, *J. Pharm. Sci. 83*, 233−238.
35. Paige, L. A., Zheng, G. Q., DeFrees, S. A., Cassady, J. M., and Geahlen, R. L. (1989) S-(-oxopentadecyl)-CoA, a nonhydrolyzable analogue of myristoyl-CoA, is a potent inhibitor of myristoyl-CoA:protein N-myristoyltransferase, *J. Med. Chem. 32*, 1665−1667.
36. Pfanner, N., Glick, B. S., Arden, S. R., and Rothman, J. E. (1990) Fatty acylation promotes fusion of transport vesicles with Golgi cisternae, *J. Cell Biol. 110*, 955−961.
37. Forman, B. M., Chen, J., and Evans, R. M. (1997) Hypolipidemic drugs, polyunsaturated fatty acids, and eicosanoids are ligands for peroxisome proliferator-activated receptors alpha and delta, *Proc. Natl. Acad. Sci. U.S.A. 94*, 4312−4317.
38. Schoonjans, K., Staels, B., and Auwerx, J. (1996) Role of the peroxisome proliferator-activated receptor (PPAR) in mediating the effects of fibrates and fatty acids on gene expression, *J. Lipid Res. 37*, 907−925.
39. Desvergne, B., and Wahli, W. (1999) Peroxisome proliferator activated receptors: nuclear control of metabolism, *Endocr. Rev. 20*, 649−688.
40. Wahli, W., Devchand, P. R., Ijpenberg, A., and Desvergne, B. (1999) in *Lipoxygenases and Their Metabolites* (Nigam and Pace-Asciak, Eds.) pp 199−209, Plenum Press, New York.
41. Escher, P., and Wahli, W. (2000) Peroxisome proliferator activated receptors: insights into multiple cellular functions, *Mutat. Res. 448*, 121−138.
42. Martin, G., Poirier, H., Nennuyer, N., Crombie, D., Fruchart, J. C., Heyman, R. A., Besnard, P., and Auwerx, J. (2000) Induction of the fatty acid transport protein 1 and acyl CoA synthase genes by dimer selective rexinoids suggests that the PPAR−RXR heterodimer is their molecular target, *J. Biol. Chem. 275*, 12612−12618.
43. Schoonjans, K., Staels, B., and Auwerx, J. (1996) Role of the peroxisome proliferator-activated receptor (PPAR) in mediating the effects of fibrates and fatty acids on gene expression, *J. Lipid Res. 37*, 907−925.
44. Lemberger, T., Desvergne, B., and Wahli, W. (1996) Peroxisome Proliferator-Activated Receptors, *Annu. Rev. Cell Dev. Biol. 12*, 335−363.
45. Seedorf, U., and Assmann, G. (2001) The role of PPARalpha in obesity, *Nutr. Metab. Cardiovasc. Dis. 11*, 189−194.
46. Kersten, S., Desvergne, B., and Wahli, W. (2000) Roles of PPARs in health and disease, *Nature 405*, 421−424.
47. Costet, P., Legendre, C., More, J., Edgar, A., Galtier, P., and Pineau, T. (1998) PPARalpha deficiency leads to progressive dyslipidemia with sexually dimorphic obesity and steatosis, *J. Biol. Chem. 273*, 29577−29585.
48. Djouadi, F., Weinheimer, C. J., Saffitz, J. E., Pitchford, C., Bastin, J., and Gonzalez, F. J. (1998) A gender-related defect in lipid metabolism and glucose homeostasis in PPARalpha deficient mice, *J. Clin. Invest. 102*, 1083−1091.

49. Kersten, S., Seydoux, J., Peters, J. M., Gonzalex, F. J., Desvergne, B., and Wahli, W. (1999) PPARalpha activates the adaptive response to fasting, *J. Clin. Invest. 103*, 1489−1498.
50. Aoyama, T., Peters, J. M., Iritani, N., Nakajima, T., Furihata, K., Hashimoto, T., and Gonzalez, F. J. (1998) Altered constitutive expression of fatty acid metabolizing enzymes in mice lacking PPARalpha, *J. Biol. Chem. 273*, 5678−5684.
51. Peters, J. M., Hennuyer, N., Staels, B., Fruchart, J. C., Fievet, C., Gonzalez, F. J., and Auwerx, J. (1997) Alterations in lipoprotein metabolism in peroxisome proliferator-activated receptor a-deficient mice, *J. Biol. Chem. 272*, 27307−27312.
52. Naiki, T., Nagaki, M., Shidoji, Y., Kojima, H., Imose, M., Kato, T., Ohnishi, N., Yagi, K., and Moriwaki, H. (2002) Analysis of gene expression profile induced by hepatocyte nuclear factor 4alpha in hepatoma cells using an oligonucleotide microarray, *J. Biol. Chem. 277*, 14011−14019.
53. Hertz, R., Magenheim, J., Berman, I., and Bar-Tana, J. (1998) Fatty acyl-CoA thioesters are ligands of hepatic nuclear factor-4alpha, *Nature 392*, 512−516.
54. Jiang, G., Nepomuceno, L., Hopkins, K., and Sladek, F. M. (1995) Exclusive homodimerization of the orphan receptor hepatocyte nuclear factor 4 defines a new subclass of nuclear receptors, *Mol. Cell. Biol. 15*, 5131−5134.
55. Hadzopoulou-Cladaras, M., Kistanova, E., Evagelopoulou, C., Zeng, S., Cladaras, C., and Ladias, A. A. J. (1997) Functional Domains of the Nuclear Receptor Hepatocyte Nuclear Factor 4*, *J. Biol. Chem. 272*, 539−550.
56. Chen, W. S., Manova, K., Weinstein, D. C., Duncan, S. A., Plump, A. S., Prezioso, V. R., Bachvarova, R. F., and Darnell, J. E. (1994) Disruption of the HNF4alpha gene, expressed in visceral endoderm, leads to cell death in embryonic ectoderm and impaired gastrulation of mouse embryos, *Genes Dev. 8*, 2466−2477.
57. Shih, D. W., Dansky, H. M., Fleisher, M., Assmann, G., Fajans, S., and Stoffel, M. (2000) Genotype/phenotype relationsips in HNF-4alpha/MODY1: haploinsufficiency is associated with reduced apolipoprotein (AII), apolipoprotein (CIII), lipoprotein-(a), and triglyceride levels, *Diabetes 49*, 832−837.
58. Furuta, H., Iwasaki, N., Oda, N., Hinokio, Y., Horikawa, Y., Yamagata, K., Yano, N., Sugahiro, J., Ogata, M., Ohgawara, H., Omori, Y., Iwamoto, Y., and Bell, G. I. (1997) Organization and partial sequence of the hepatocyte nuclear factor 4alpha/MODY1 gene and indentification of a missense mutation, R127W, in a Japanese family with MODY, *Diabetes 46*, 1652−1657.
59. Herman, W. H., Fajans, S. S., Smith, M. J., Polonsky, K. S., Bell, G. I., and Halter, J. B. (1997) Diminished insulin and glucagon secretory responses to arginine in nondiabetic subjects with a mutation in the hepatocyte nuclear factor 4alpha/MODY1 gene, *Diabetes 46*, 1749−1754.
60. Lawrence, J. W., Kroll, D. J., and Eacho, P. I. (2000) Ligand dependent interaction of hepatic fatty acid binding protein with the nucleus, *J. Lipid Res. 41*, 1390−1401.
61. Kier, A. B., and Schroeder, F. (1982) Development of metastatic tumors in athymic (nude) mice from LM cells grown in vitro, *Transplantation 33*, 274−279.
62. Kier, A. B. (1990) Plasma membrane properties of cultured local LM cell tumors and metastases from athymic (nude) mice, *Cancer Lett. 50*, 19−30.
63. Kier, A. B. (1990) Membrane properties of metastatic and nonmetastatic cells cultured from C3H mice injected with LM fibroblasts, *Biochim. Biophys. Acta 1022*, 365−372.
64. Gorski, J., Nawrocki, A., and Murthy, M. (1998) Characterization of free and glyceride-esterified long chain fatty acids in different skeletal muscle types of the rat, *Mol. Cell. Biochem. 178*, 113−118.
65. Nawrocki, A., Gorska, M., Zendzian-Piotrowska, M., and Gorski, J. (1999) Effect of acute streptozotocin diabetes on fatty acid content and composition in different lipid fractions of rat skeletal muscle, *Horm. Metab. Res. 31*, 252−256.
66. Gorski, J., Zendzian-Piotrowska, M., Wolfrum, C., Nawrocki, A., and Spener, F. (2000) Effect of sex and bezafibrate on incorporation of blood borne palmitate into lipids of rat liver nuclei, *Mol. Cell. Biochem. 214*, 57−62.
67. Gossett, R. E., Frolov, A. A., Roths, J. B., Behnke, W. D., Kier, A. B., and Schroeder, F. (1996) Acyl Co A binding proteins: multiplicity and function, *Lipids 31*, 895−918.
68. Elholm, M., Garras, A., Neve, S., Tarnehave, D., Lund, T. B., Skorve, J., Flatmark, T., Kristiansen, K., and Berge, R. K. (2000) Long chain acyl CoA esters and acyl CoA binding protein are present in the nucleus of rat liver cells, *J. Lipid Res. 41*, 538−545.
69. Knudsen, J. (1990) Acyl-CoA-binding protein (ACBP) and its relation to fatty acid-binding protein (FABP): an overview, *Mol. Cell. Biochem. 98*, 217−223.
70. Murphy, E. J. (1998) L-FABP and I-FABP expression increase NBD-stearate uptake and cytoplasmic diffusion in L-cells, *Am. J. Physiol. 38*, G244−G249.
71. Luxon, B. A., and Weisiger, R. A. (1993) Sex differences in intracellular fatty acid transport: role of cytoplasmic binding proteins, *Am. J. Phys. 265*, G831−G841.
72. Knudsen, J., Jensen, M. V., Hansen, J. K., Faergeman, N. J., Neergard, T., and Gaigg, B. (1999) Role of acyl CoA binding protein in acyl CoA transport, metabolism, and cell signaling, *Mol. Cell. Biochem. 192*, 95−103.
73. Faergeman, N. J., and Knudsen, J. (1997) Role of long-chain fatty acyl-CoA esters in the regulation of metabolism and in cell signaling, *Biochem. J. 323*, 1−12.
74. Frolov, A. A., and Schroeder, F. (1998) Acyl coenzyme A binding protein: conformational sensitivity to long chain fatty acyl-CoA, *J. Biol. Chem. 273*, 11049−11055.
75. Wadum, M. C. T., Villadsen, J. K., Feddersen, S., Moller, R. S., Neergaard, T. B. F., Kragelund, B. B., Hojrup, P., Faergeman, N. J., and Knudsen, J. (2002) Fluorescently labeled bovine acyl CoA binding protein acting as an acyl CoA sensor: interaction with CoA and acyl CoA esters and its use in measuring free acyl CoA esters and nonesterified fatty acids, *Biochem. J. 365*, 165−172.
76. Mandrup, S., Jepsen, R., Skott, H., Rosendal, J., Hojrup, P., Kristiansen, K., and Knudsen, J. (1993) Effect of heterologous expression of acyl-CoA-binding protein on acyl-CoA level and composition in yeast, *Biochem. J. 290*, 369−374.
77. Starodub, O., Jolly, C. A., Atshaves, B. P., Roths, J. B., Murphy, E. J., Kier, A. B., and Schroeder, F. (2000) Sterol carrier protein-2 immunolocalization in endoplasmic reticulum and stimulation of phospholipid formation, *Am. J. Physiol. 279*, C1259−C1269.
78. Rasmussen, J. T., Rosendal, J., and Knudsen, J. (1993) Interaction of acyl-CoA binding protein (ACBP) on processes for which acyl-CoA is a substrate, product or inhibitor, *Biochem. J. 292*, 907−913.
79. Keenan, T. W., Bereszney, R., Funk, L. K., and Crane, F. L. (1970) Lipid composition of nuclear membranes isolated from bovine liver, *Biochim. Biophys. Acta 203*, 547−554.
80. Kleinig, H. (1970) Nuclear membranes from mammalian liver, *J. Cell Biol. 96*, 396−402.
81. Keler, T., Khan, S. H., and Sorof, S. (1997) Liver fatty acid binding protein and mitogenesis in transfected hepatoma cells, *Adv. Exp. Med. Biol. 400A*, 517−524.
82. Lawrence, J. W., Li, Y., Chen, S., Deluca, J. G., Berger, J. P., Umbenhauer, D. R., Moller, D. E., and Zhou, G. (2001) Differential gene regulation in human versus rodent hepatocytes by peroxisome proliferator-activated receptor (PPAR)alpha. PPAR-alpha fails to induce peroxisome proliferation-associated genes in human cells independently of the level of receptor expression, *J. Biol. Chem. 276*, 31521−31527.
83. Mizushina, Y., Sugawara, F., Iida, A., and Sakaguchi, K. (2000) Structural homology between DNA binding sites of DNA polymerase beta and DNA topoisomerase II, *J. Mol. Biol. 304*, 385−395.
84. Mizushima, Y., Sagisaka, M., Sakaib, H., Abeb, M., and Sakaguchi, K. (2000) Mode analysis of binding of fatty acids to mammalian DNA polymerases, *Biochim. Biophys. Acta 1486*, 211−218.

BI0352318